

Pyronaridine Protects against SARS-CoV-2 Infection in Mouse

Ana C. Puhl,^{*,#} Giovanni F. Gomes,[#] Samara Damasceno, Andre S. Godoy, Gabriela D. Noske, Aline M. Nakamura, Victor O. Gawriljuk, Rafaela S. Fernandes, Natalia Monakhova, Olga Riabova, Thomas R. Lane, Vadim Makarov, Flavio P. Veras, Sabrina S. Batah, Alexandre T. Fabro, Glaucius Oliva, Fernando Q. Cunha, José C. Alves-Filho, Thiago M. Cunha,^{*} and Sean Ekins^{*}



Cite This: <https://doi.org/10.1021/acscinfecdis.2c00091>



Read Online

ACCESS |



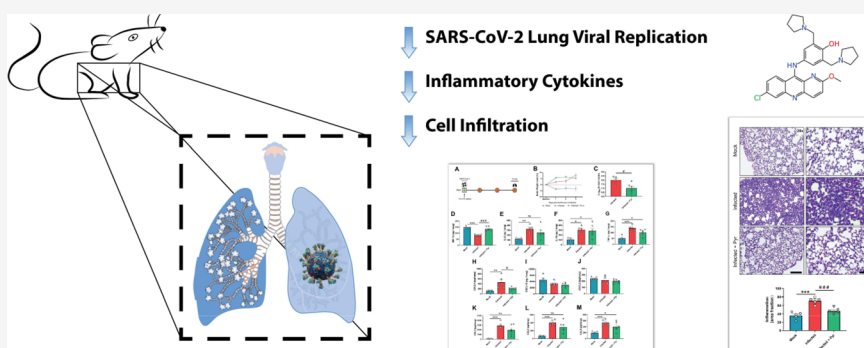
Metrics & More



Article Recommendations



Supporting Information



ABSTRACT: There are currently relatively few small-molecule antiviral drugs that are either approved or emergency-approved for use against severe acute respiratory coronavirus 2 (SARS-CoV-2). One of these is remdesivir, which was originally repurposed from its use against Ebola. We evaluated three molecules we had previously identified computationally with antiviral activity against Ebola and Marburg and identified pyronaridine, which inhibited the SARS-CoV-2 replication in A549-ACE2 cells. The *in vivo* efficacy of pyronaridine has now been assessed in a K18-hACE transgenic mouse model of COVID-19. Pyronaridine treatment demonstrated a statistically significant reduction of viral load in the lungs of SARS-CoV-2-infected mice, reducing lung pathology, which was also associated with significant reduction in the levels of pro-inflammatory cytokines/chemokine and cell infiltration. Pyronaridine inhibited the viral PL^{P_{ro}} activity *in vitro* (IC₅₀ of 1.8 μ M) without any effect on M^{P_{ro}}, indicating a possible molecular mechanism involved in its ability to inhibit SARS-CoV-2 replication. We have also generated several pyronaridine analogs to assist in understanding the structure activity relationship for PL^{P_{ro}} inhibition. Our results indicate that pyronaridine is a potential therapeutic candidate for COVID-19.

KEYWORDS: antiviral, SARS-CoV-2, spike protein, pyronaridine

There is currently intense interest in discovering small molecules with direct antiviral activity against the severe acute respiratory syndrome coronavirus 2 (SARS-CoV-2). Pyronaridine, an antiviral drug with *in vitro* activity against Ebola, Marburg, and SARS-CoV-2, has now statistically significantly reduced the viral load in mice along with TNF- α , CXCL1, and CCL3 and restored levels of IFN-1 β , ultimately demonstrating a protective effect against lung damage by infection to provide a new potential treatment for testing clinically.

At the time of writing, we are in the midst of a major global health crisis caused by the virus severe acute respiratory syndrome coronavirus 2 (SARS-CoV-2) that was originally reported in Wuhan, China in late 2019.^{1,2} Infection with this virus leads to extensive morbidity, mortality, and a very broad range of clinical symptoms such as cough, loss of smell and taste, respiratory distress, pneumonia, and extrapulmonary

events characterized by a sepsis-like disease collectively called 2019 coronavirus disease (COVID-19).³ In the United States, there are currently three vaccines available, one of which has recently obtained with full approval from the Food and Drug Administration (FDA) to protect against SARS-CoV-2.^{4–6} There are however few small-molecule drugs approved for COVID-19,⁷ including remdesivir,⁸ which originally demonstrated activity in Vero cells,^{9,10} human epithelial cells, and in Calu-3 cells¹⁰ infected with SARS-CoV-2 prior to clinical

Received: February 11, 2022



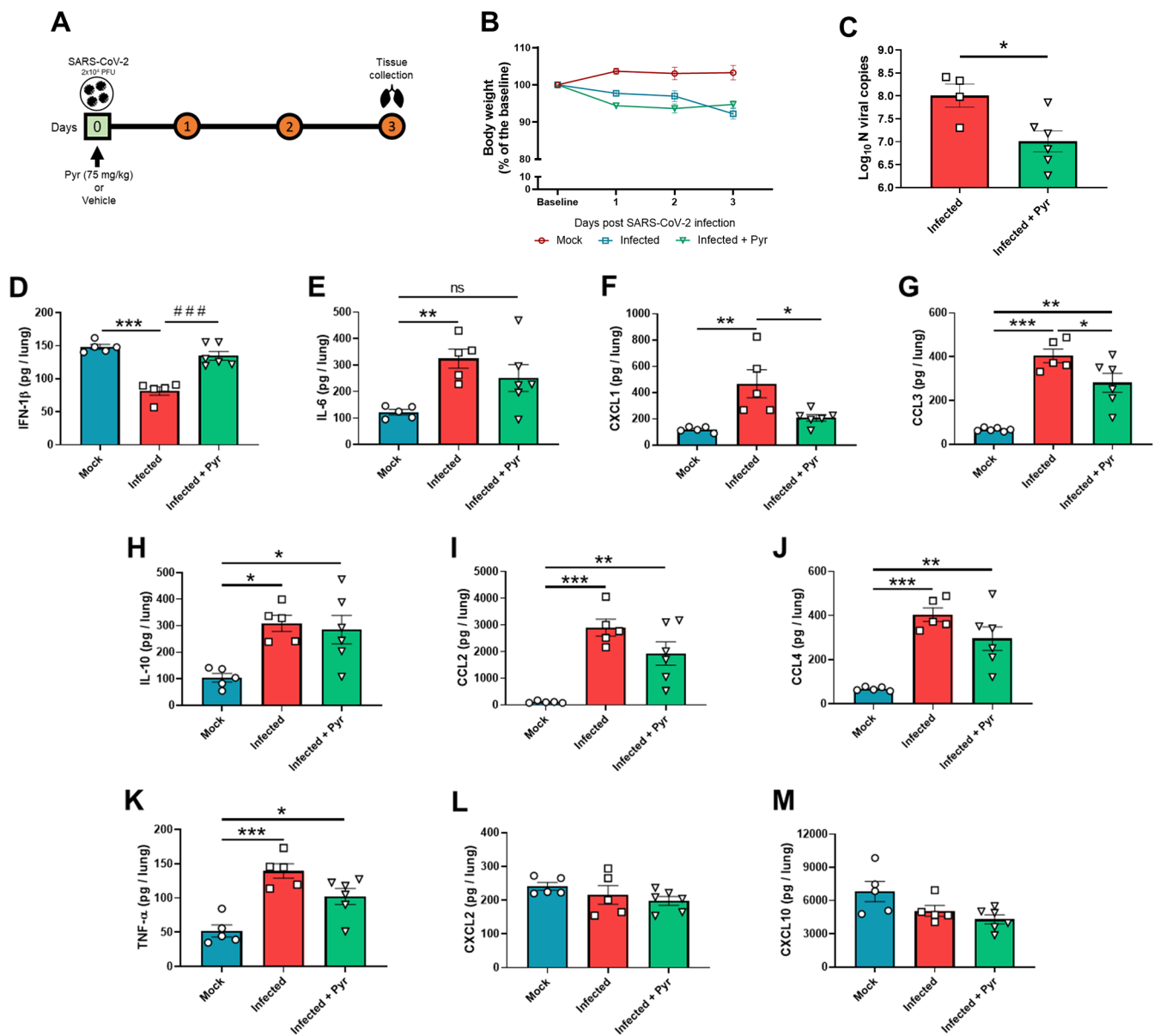


Figure 1. *In vivo* efficacy of pyronaridine in a mouse model of COVID-19. (A) Experimental timeline: K18-hACE2 mice were infected with SARS-CoV-2 (2×10^4 PFU/40 μ L of saline, intranasal) or mock. One group of mice was treated with pyronaridine (75 mg/kg i.p.) 1 h before virus inoculation. (B) Body weight was evaluated daily. (C) At 3 DPI, mice were euthanized and the lung viral load and (D–M) lung cytokine and chemokine levels were determined. * $p < 0.05$, ** $p < 0.01$, and *** $p < 0.001$ after one-way ANOVA followed by Tukey post-hoc test. Pyr, pyronaridine.

testing. Remdesivir represents a repurposed drug that was originally developed for Hepatitis C virus but was then repurposed for treating Ebola and has since reached clinical trials.¹¹

We therefore hypothesized that other drugs that were effective against Ebola might also be prioritized for evaluation *in vitro* against SARS-CoV-2. Previously, we had used a machine-learning model to identify tilorone, quinacrine, and pyronaridine tetraphosphate¹² for testing against Ebola virus (EBOV), and subsequently, these three inhibited EBOV and Marburg *in vitro* as well as demonstrating significant efficacy in the mouse-adapted EBOV (ma-EBOV) model.^{13–15} All of these molecules were identified as lysosomotropic, a characteristic that suggests that these could be possible entry inhibitors.¹⁶ Pyronaridine tetraphosphate is used as an antimalarial in several countries as part of a combination

therapy with artesunate (Pyramax). Pyronaridine alone also demonstrated significant activity in the guinea pig-adapted model of EBOV infection.¹⁷ We and others^{18–21} have recently shown that these compounds possess *in vitro* activity against SARS-CoV-2, and tilorone and pyronaridine are in clinical trials, the latter in combination with artesunate. The C_{max} data for pyronaridine in our previous mouse pharmacokinetics studies (i.p. dosing) suggests that plasma levels that are above the average IC_{50} observed for SARS-CoV-2 inhibition *in vitro*¹³ can be reached with dosing well below the maximum tolerated dose. Pyronaridine also has excellent *in vitro* ADME properties with a long half-life that makes a single-dose treatment possible.^{13,18} We now expand on our earlier *in vitro* characterization of pyronaridine¹⁸ by assessing the *in vivo* efficacy in a mouse model of COVID-19. Finally, in an attempt

to further explore molecular mechanisms, we tested the activity of pyronaridine *in vitro* against viral and host targets.

RESULTS AND DISCUSSION

In vivo efficacy was assessed in the K18-hACE2 mouse model of COVID-19.^{22–24} Pyronaridine (75 mg/kg, i.p.)¹³ was administered 1 h prior to infection. Mice that were given pyronaridine received a single treatment. On the third day post-infection, mice were euthanized and lung viral load, cytokine levels, and histopathology were evaluated (Figure 1A). We chose day 3 post-infection since it is the time point of the highest viral load in the lung of K18-hACE2 mice infected with SARS-CoV-2.^{23,25,26} In all groups tested, mice lost weight compared to uninfected animals that received only vehicle formulation (Figure 1B). Lung viral load was evaluated by RT-qPCR, and the pyronaridine-treated group showed a statistically significant decrease in the lung viral load (Figure 1C). Moreover, reduced levels of IFN-1 β were observed in infected mice, and pyronaridine restored the levels of IFN-1 β close to that found in uninfected animals (Figure 1D). Tukey post-hoc analysis revealed a significant increase in IL-6 levels in infected untreated mice as compared with the uninfected group (uninfected vs infected untreated) (Figure 1E). Interestingly, we observed no post-hoc difference when comparing pyronaridine-treated infected mice with the uninfected group (uninfected vs infected + pyr) (Figure 1E). In addition, pyronaridine reduced the high levels of CXCL1 and CCL3 observed in infected animals (Figure 1F and Figure 1G, respectively). Pyronaridine did not, however, reduce the high levels of IL-10, CCL2, CCL4, and TNF- α (Figure 1H–K, respectively) below the elevated levels found in the infected mice. Neither infection nor treatment affected the levels of CXCL2 and CXCL10 (Figure 1L and Figure 1M, respectively).

Several studies have shown a cytokine and chemokine storm as important during SARS-CoV-2 infection in patients with COVID-19, including PDGF, VEGF,²⁷ IL-6,^{28,29} IL-8, IL-10,²⁹ TNF- α ,²⁹ IFN- α , and IFN- β .^{30–34} Furthermore, an impaired type I interferon response has already been observed in COVID-19³⁵ followed by increased circulating levels of IL-6 and TNF- α . Many viruses, including SARS-CoV-2, subvert the immune system by inhibiting the production of interferons (IFN), an important family of antiviral mediators,^{36–39} which results in an impaired antiviral defense and increased viral replication and infection. Here, we have demonstrated that pyronaridine restored the levels of IFN-1 β in infected mice. Moreover, this effect was associated with a reduced viral load after the treatment with pyronaridine. Notably, pyronaridine also reverted the altered levels of CXCL1 and CCL3 observed in infected mice, in addition to avoiding the increase in the levels of IL-6 noticed in individuals infected with SARS-CoV-2. Noteworthy, we did not observe changes in the levels of CXCL10 post SARS-CoV-2 infection, as previously reported.²³ Although discrepant, this difference could be explained by the higher viral inoculum used in the previous study (1×10^5 PFU) in comparison to 2×10^4 PFU used here. Moreover, the difference in the time points after infection could be also a possible explanation. In fact, Oladunni et al.²³ observed increased CXCL10 on 2 dpi decreasing thereafter.

In addition to biochemical changes, histopathological findings are also observed in the lung of patients^{40–42} and in other experimental models of COVID-19.^{22–24} To determine the severity of lung damage, histological examination of

hematoxylin and eosin (H&E)-stained lung tissues was performed. Infected, untreated mice showed severe pathological changes with inflammatory cell infiltrates. In contrast, pyronaridine-treated animals exhibited improved morphology and milder infiltration, appearing comparable to those of uninfected mice (Figure 2A). Histological observations were

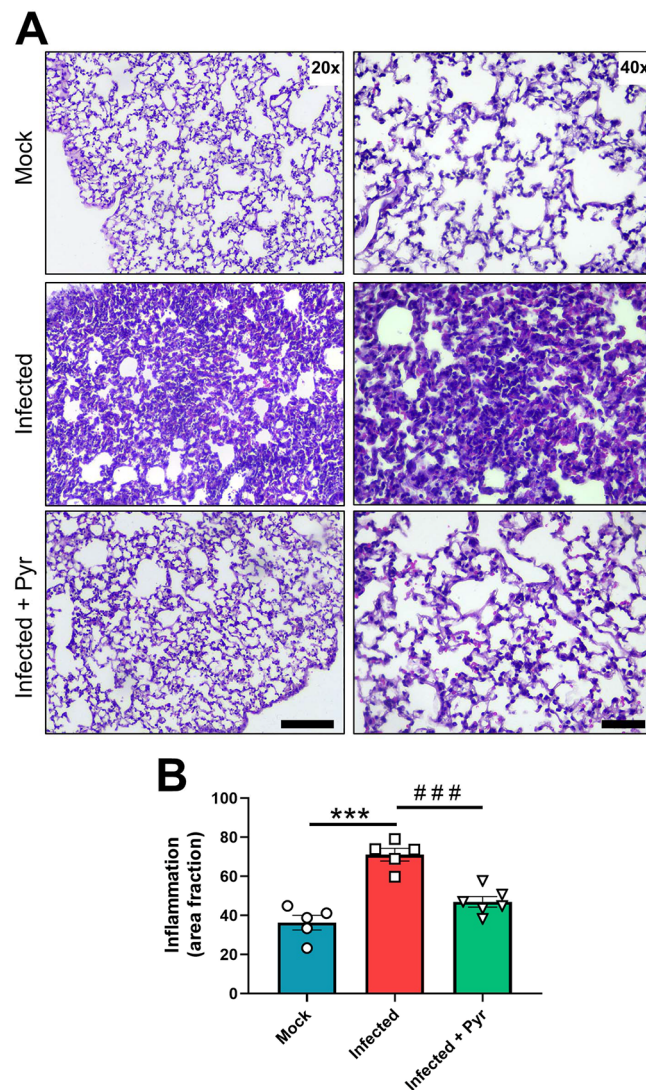


Figure 2. Lung histopathological analyses of COVID-19 mice treated with pyronaridine. K18-hACE2 mice were infected with SARS-CoV-2 (2×10^4 PFU/40 μ L, intranasal) or mock. One group of mice was treated with pyronaridine (75 mg/kg i.p.) 1 h before virus inoculation. At 3 DPI, mice were euthanized, and the lungs were harvested and processed for histopathological analyses. (A) Representative images of lung slices stained with hematoxylin and eosin (H&E). (B) Quantitative morphometric analyses based on the septal area fraction. *** $p < 0.001$ after one-way ANOVA followed by Tukey post-hoc test. Pyr, pyronaridine. Scale bars: 20 \times = 125 μ m; 40 \times = 50 μ m.

confirmed by quantitative morphometric analysis of the H&E-stained slides showing a statistically significant reduction in inflammation (Figure 2B). Thus, pyronaridine appears to have both antiviral and immunomodulatory effects in this experimental model of COVID-19 as used in the present study.

SARS-CoV-2 proteases M^{Pro} and PL^{Pro} are essential for viral replication and have been widely studied for the discovery of new direct acting antivirals.^{43–45} The FDA approved the

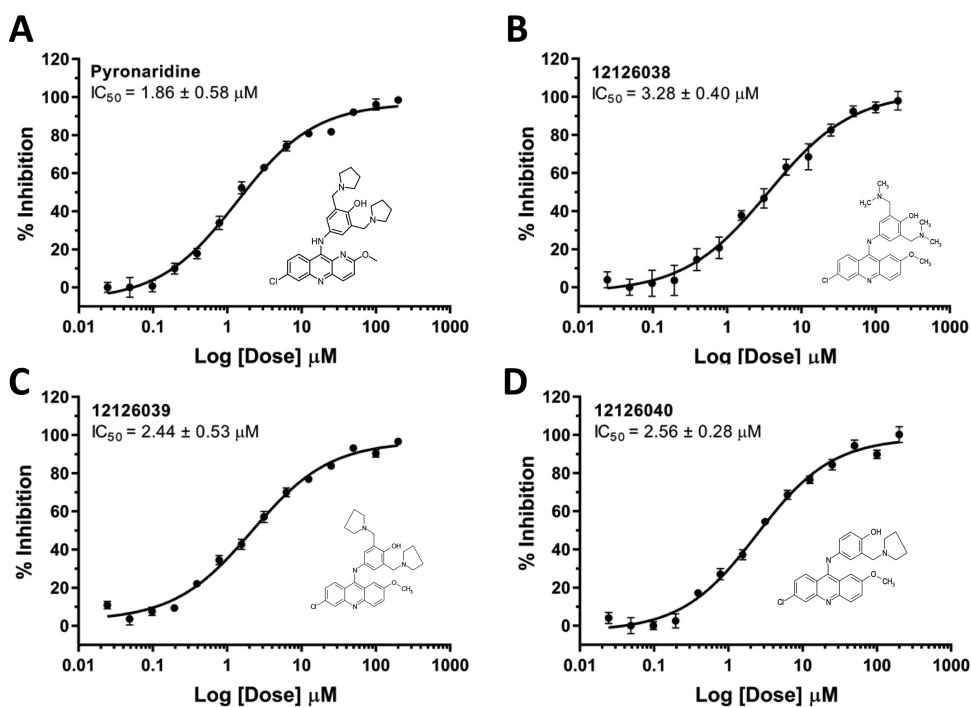


Figure 3. Dose–response curves of pyronaridine and active analogs against SARS-CoV-2 PL^{pro}. (A) Pyronaridine, (B) 12126038, (C) 12126039, and (D) 12126040.

emergency use authorization of Pfizer’s Paxlovid, which is a combination of PF-07321332 and the HIV drug ritonavir that slows down the metabolism of PF-07321332 to treat mild-to-moderate COVID-19 in adults and pediatric patients 12 years of age and older (www.fda.gov). PF-07321332 is an M^{pro} inhibitor. Currently, there are no PL^{pro} inhibitors approved to treat COVID-19.

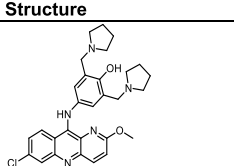
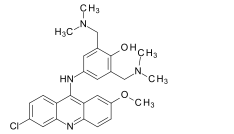
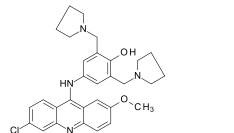
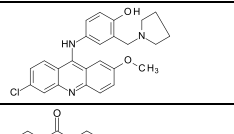
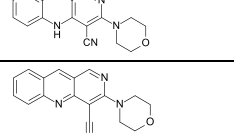
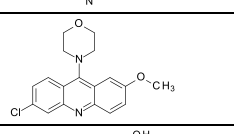
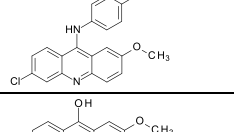
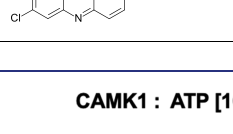

Pyronaridine was therefore tested against both SARS-CoV-2 recombinant PL^{pro} and M^{pro} through fluorescence resonance energy transfer (FRET)-based *in vitro* assays. Pyronaridine inhibited PL^{pro} with an IC₅₀ of 1.86 ± 0.58 μM (Figure 3A) but did not show any appreciable activity against M^{pro} at 20 μM (data not shown). As a positive control for M^{pro}, we used the characterized inhibitor nirmatrelvir (PF-07321332),⁴⁶ and as a positive control for PL^{pro}, we used the characterized inhibitor 15c⁴⁷ and described IC₅₀ values comparable to published data (Figure S1). Additional analogs of pyronaridine were also synthesized and tested against PL^{pro}. The analogs 12126038, 12126039, and 12126040 (Figure 3B–D, respectively) showed similar inhibitory activity when compared with pyronaridine (as well as that reported for GRL0617⁴⁸), indicating that the aminophenol moiety together with pyrrole or tertiary amine substitutions at the meta position is tolerated for PL^{pro} inhibition (Table 1 and Figure 3A). The deletion of these groups in analogs 10326099, 12126035, 12126036, 12126037, and 12126072 caused complete abolishment of the inhibitory activity of the series (Table 1). The PL^{pro} active site contains four subsites for peptide recognition, with a strong preference for positively charged amino acids at P3 and P4 subsites.^{43–45} There are only a few PL^{pro} inhibitors reported to date, such as daclastavir and sitagliptin with low micromolar IC₅₀ for PL^{pro}⁴⁹ and GRL0617,⁴⁸ for which the crystal structure and binding mode have been reported. Recently, novel 2-phenylthiophenes with nanomolar inhibitory potency were

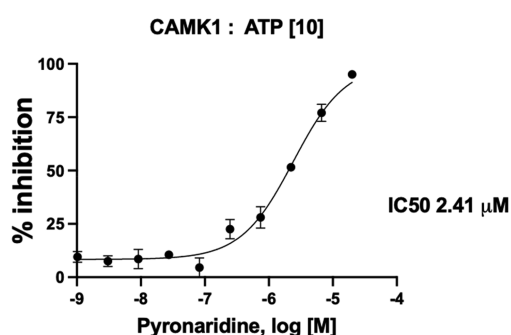
designed by leveraging the cooperativity of multiple shallow binding sites on the PL^{pro} surface.⁵⁰

Due to the possible effect of pyronaridine on cytokines (Figure 1), we have also assessed the effect on host targets as SARS-CoV-2 can cause an imbalance in the immune system that may result in a cytokine storm⁵¹ as well as leading to acute respiratory distress syndrome (ARDS), coagulation disorders, and eventually multiple organ failure.^{51,52} Hence, targeting the cytokine storm to address hyperinflammation represents another approach to the treatment of COVID-19 patients.^{53–56} In this regard, we have explored the effect of pyronaridine on human kinases, which are responsible for host cell signaling.^{57,58} Screening of pyronaridine (tested at 1 μM) against 485 kinases identified only two as having a mean percent inhibition greater than 30%, including CAMK1 (35%) and MELK (31%) (Table S1). Subsequently, the IC₅₀ was determined for CAMK1 (2.4 μM) (Figure 4).

Even with vaccines becoming widely available in many countries, COVID-19 continues to exact a very heavy toll on those that are unvaccinated. We are in a race against time before the virus mutates, and vaccines lose their effectiveness. There is therefore an urgent need for new antivirals and in particular small-molecule treatments that are orally delivered and can be used outside of a hospital setting. Finding, developing, and progressing small molecules to the clinic are generally slow and expensive processes;⁵⁹ hence, drug repurposing has been attempted by many groups to speed these up (either experimentally or computationally⁶⁰) by identifying already approved or clinical stage candidates used for other applications or quickly follow up the few molecules that are being used already. The traditional prioritization of compounds *in vitro* before animal models and then humans is still repeated and so far with few successes with many molecules not demonstrating efficacy *in vivo*.^{61,62}

Table 1. PL^{pro} IC₅₀ Inhibition Data for Pyronaridine Analogs

Molecule	Structure	Mol wt	IC ₅₀ (μM)
Pyronaridine		518.05	1.86 ± 0.58
12126038		465.00	3.28 ± 0.4
12126039		517.08	2.44 ± 0.53
12126040		433.94	2.56 ± 0.28
10326099		306.33	>20
12126035		290.33	>20
12126036		328.80	>20
12126037		350.81	>20
12126072		259.69	>20

**Figure 4.** Pyronaridine CAMK1 dose response.

Our understanding of the antiviral mechanism of pyronaridine previously shown to inhibit the Ebola virus *in vitro* and *in vivo*¹³ via binding to the viral glycoprotein¹⁶ as well as through its potent lysosomotropic activity⁶³ and now the *in vitro* activity against SARS-CoV-2¹⁸ is also further expanded. Pyronaridine was previously identified with *in vitro* activity against SARS-CoV-2 in A549-ACE2 cells that was on a par with remdesivir in this cell line.¹⁸ In the current study, we have demonstrated that pyronaridine also has antiviral activity

against SARS-CoV-2 *in vivo*. A single prophylactic dose of pyronaridine (75 mg/kg i.p.) reduced the viral load in the lung of infected mice 3 days post-infection. *In vitro* assays suggest that pyronaridine possesses a direct antiviral effect showing activity against PL^{pro} (IC₅₀ = 1.86 μM; Figure 3A) but did not inhibit SARS-CoV-2 M^{pro}. Kinase profiling resulted in determination of IC₅₀ for CAMK1 (IC₅₀ = 2.4 μM; Figure 4).

A single dose (75 mg/kg i.p.) of pyronaridine has an elimination half-life of 146 h in mice,¹³ comparable to the reported half-life of pyronaridine in humans of 195–251 h.^{64,65} A study of pyronaridine as a single-oral dose (400 mg) given to a healthy volunteer found a C_{max} in plasma of 495.8 ng/mL at a T_{max} of 0.5 h,^{64,66} which gives a concentration close to 1 μM. In our study, pyronaridine inhibits PL^{pro} at 1.86 μM and CAMK1 at 2.4 μM, which is very close to a C_{max} of 1 μM. Pyronaridine preferentially associates with blood cells and is highly plasma protein bound,⁶⁶ which suggests that it may not reach the unbound concentration necessary to have an effect on PL^{pro} and CAMK1 at these doses. Activation of CAMK1 has been reported to negatively impact HBV biosynthesis.^{67,68} Inhibition of CAMK1 might not however be therapeutically relevant since reports on proteomic and phosphoproteomic profiling of COVID-19⁶⁹ and phosphorylation landscape for SARS-CoV-2 infection⁷⁰ do not point to an important role of this kinase on COVID-19. Currently, Shin Poong Pharmaceutical Co. Ltd. is recruiting patients for phase III clinical trials for COVID-19 (ClinicalTrials.gov Identifier: NCT05084911) using a combination of pyronaridine and artesunate. In phase II, this combination showed some promising effects in those with severe illness.⁷¹

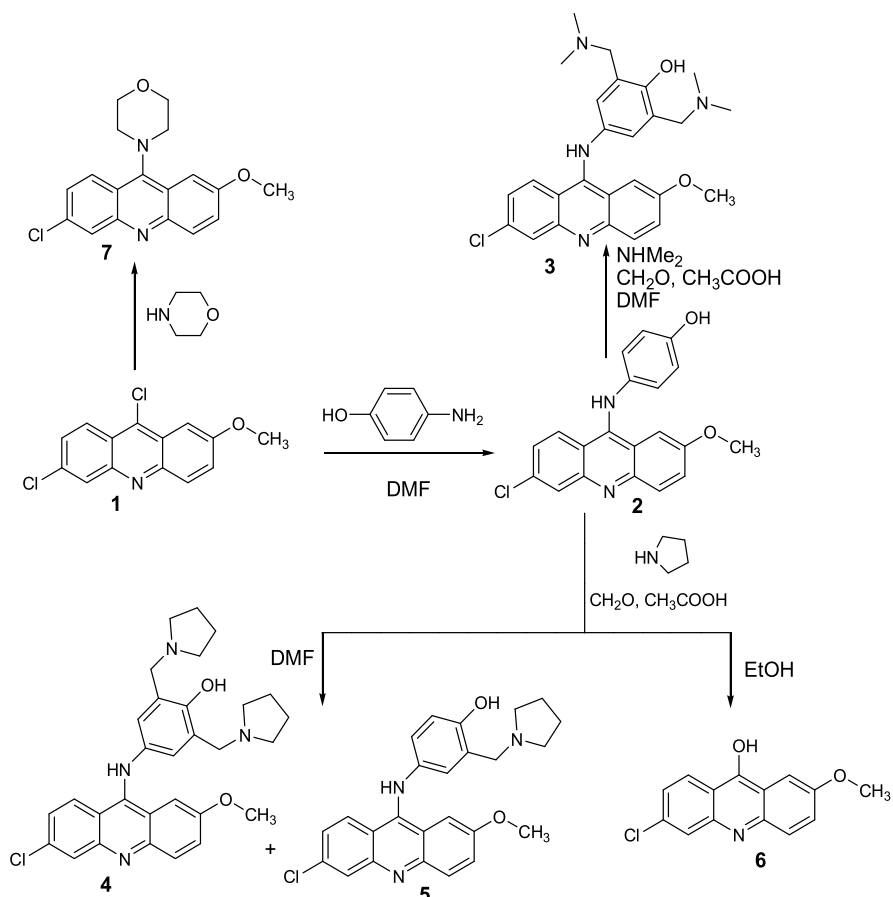
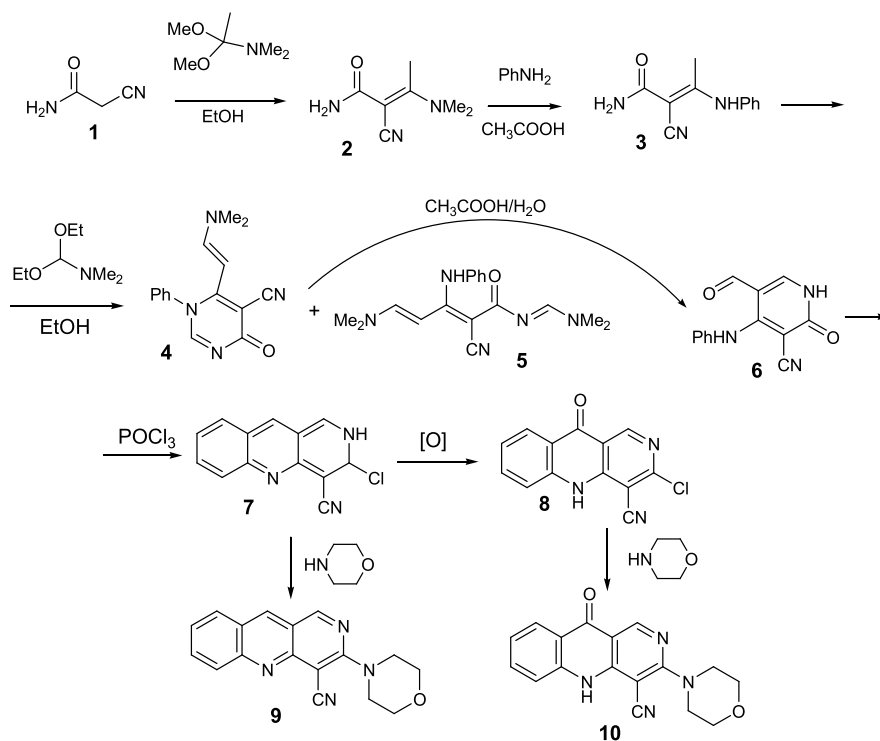
In summary, our present study provided additional data on the efficacy of pyronaridine against SARS-CoV-2 infection as well as highlighting reduced lung pathology and inflammation in a mouse model of COVID-19. Furthermore, we have shown that pyronaridine may target PL^{pro} as well as CAMK1. There are few inhibitors of CAMK1 that have been identified to date (such as Baretin⁷² or pyridine amides⁷³), which have a role in inflammation targeting IL-10.⁷² Previous *in vitro* work has shown that inhibiting CAMK1 in cells reduces IL-10, the master anti-inflammatory interleukin.⁷⁴ In the present study, there is no significant difference in the IL-10 levels between the untreated and pyronaridine-treated infected groups so it seems unlikely that CAMK1 inhibition would be involved in the mechanism of action of inhibition of SAR-CoV-2. In conclusion, we propose that pyronaridine could be used alone as a potential therapeutic candidate for COVID-19. Finally, with the emerging virulence of novel SARS-CoV-2 strains, identifying repurposed drugs with novel mechanisms of action and whose antiviral activity translates from *in vitro* to *in vivo* is rare⁶² and may lead to new treatments as well as their further optimization.

METHODS

Chemicals and Reagents. Compound 15c⁴⁷ was purchased from Sigma-Aldrich. Nirmatrelvir (PF-07321332)⁴⁶ was kindly donated by Prof. Carlos Alberto Montanari (University of São Paulo, Brazil).

Pyronaridine tetraphosphate [4-[(7-chloro-2-methoxybenzo-*[b]*[1,5]naphthyridin-10-yl)amino]-2,6-bis(1-pyrrolidinylmethyl)phenol phosphate (1:4)]¹² was purchased from BOC Sciences (Shirley, NY). The purity of this compound was greater than 95%. For pyronaridine analogs, ¹H and ¹³C spectra were measured on Bruker AC-300 (300

Scheme 1. Synthetic Route for 6-Chloro-2-methoxyacridine Derivatives

Scheme 2. Synthetic Route for Benzo[*b*]-1,6-naphthyridine Derivatives

MHz, ^1H) or Bruker AC-200 (50 MHz, ^{13}C). Chemical shifts were measured in $\text{DMSO-}d_6$ or CDCl_3 using tetramethylsilane

as an internal standard and reported as unit (ppm) values. The following abbreviations are used to indicate the multiplicity: s,

singlet; d, doublet; t, triplet; m, multiplet; dd, doublet of doublets; brs, broad singlet; and brm, broad multiplet. The purity of the final compounds was analyzed on an Agilent 1290 Infinity II HPLC system coupled to an Agilent 6460 triple-quadrupole mass spectrometer equipped with an electrospray ionization source. The chromatographic separation was carried out on an Agilent Eclipse Plus C18 RRHD column (2.1 × 50 mm, 1.8 μm) at 40 °C, and the sample injection volume was 0.2 μL. The mobile phase comprising 0.1% formic acid/water (A) and 0.1% formic acid and 85% acetonitrile/water (B) was programmed with gradient elution (0.0–3.0 min, 60% B; 3.0–4.0 min, 60–97% B; 4.0–6.0 min, 97% B; 6.0–6.1 min, 97–60% B) at a flow rate of 0.4 mL/min. The mass spectrometric detection was operated in positive ion mode. Optimal parameters were capillary voltages of 3500 V, a nebulizer pressure of 35 psi, a gas temperature of 350 °C, and a gas flow rate of 12 L/min. All final compounds are >95% pure. Melting points were determined on Electrothermal 9001 (10 °C per min) and are uncorrected. Merck KGaA silica gel 60 F₂₅₄ plates were used for analytical thin-layer chromatography. Column chromatography was performed on Merck silica gel 60 (70–230 mesh). Yields refer to purified products and are not optimized.

The molecules were synthesized, according to Schemes 1 or 2, and the specific methods and analytical results are described in the Supporting Information.

Test Article Preparation. Dose formulation for pyronaridine was prepared as previously described¹³ under yellow light by mixing the appropriate amount of pyronaridine in melted Kolliphor HS 15 (Solutol) (20% final volume) using a vortex mixer for 30 s. The remaining sterile water (Gibco) was added, and the formulations were mixed using a vortex mixer for 30 s to 5 min until the compound was visually dissolved and then sonicated for 25 min. The final 20% Kolliphor HS 15 dose formulations were observed to be clear, reddish solutions.

Mouse Studies. Ethical Approval. All the experimental procedures were performed in accordance with the guide for the use of laboratory animals of the University of São Paulo and approved by the institutional ethics committee under the protocol number 105/2021.

SARS-CoV-2 Isolate. SARS-CoV-2 was isolated from a COVID-19 positive-tested patient. The virus was propagated and titrated in Vero E6 cells in a biosafety level 3 laboratory (BSL3) at the Ribeirão Preto Medical School (Ribeirão Preto, Brazil). Cells were cultured in a DMEM medium supplemented with 10% fetal bovine serum (FBS) and antibiotic/antimycotic (Penicillin, 10,000 U/mL; Streptomycin, 10,000 μg/mL). The viral inoculum was added to Vero cells in DMEM 2% FBS and incubated at 37 °C with 5% CO₂ for 48 h. The cytopathogenic effect (CPE) was observed under a microscope. The cell monolayer was collected, and the supernatant was stored in –70 °C. Virus titration was made by the plaque-forming units (PFU).

K18-hACE2 Mice. To evaluate the effects of pyronaridine *in vivo*, we infected the K18-hACE2 humanized mice (B6.Cg-Tg(K18-ACE2)2PrImn/J).^{22–24} K18-hACE2 mice were obtained from the Jackson Laboratory and were bred in the Centro de Criação de Animais Especiais (Ribeirão Preto Medical School/University of São Paulo). This mouse model for SARS-CoV-2-induced disease has been used as it presents clinical signs and biochemical and histopathological changes compatible with the human disease.^{23–25,75–78} Mice had access

to water and food *ad libitum*. For the experimental infection, animals were transferred to the BSL3 facility.

SARS-CoV-2 Experimental Infection and Treatments. Female K18-hACE2 mice, 8 weeks old, were infected with 2×10^4 PFU of SARS-CoV-2 (in 40 μL) by the intranasal route. Uninfected mice ($N = 5$) were inoculated with an equal volume of PBS (phosphate buffered saline: 137 mM NaCl, 2.7 mM KCl, 10 mM Na₂HPO₄, 1.8 mM KH₂PO₄; pH 7.4). On the day of infection, 1 h before virus inoculation, animals were treated with pyronaridine (75 mg/kg, i.p.) ($n = 6$). Five infected animals remained untreated. Body weight was evaluated on the baseline and on all the days post-infection. On day 3 post-infection, animals were humanely euthanized, and lungs were collected. The right lung was collected, harvested, and homogenized in PBS with steel glass beads. The homogenate was added to the TRIzol (Invitrogen, CA, EUA) reagent (1:1), for posterior viral titration via RT-qPCR, or to lysis buffer (1:1), for the ELISA assay, and stored at –70 °C. The left lung was collected in paraformaldehyde (PFA 4%) for posterior histological assessment.

Absolute Viral Copy Quantification. Total RNA from the right lungs was obtained using the Trizol (Invitrogen, CA, EUA) method and quantified using NanoDrop One/OneC (Thermo Fisher Scientific, USA). A total of 800 ng of RNA was used to synthesize cDNA using a high-capacity cDNA reverse transcription kit (Applied Biosystems, Foster City, CA, USA), following the manufacturer's protocol. The determination of the absolute number of viral copies was made by a Taqman real-time qPCR assay with the aid of a StepOne real-time PCR system (Applied Biosystems, Foster City, CA, USA). A standard curve was generated to obtain the exact number of copies in the tested sample using an amplicon containing 944 bp cloned from a plasmid (PTZ57R/T CloneJet Cloning Kit Thermo Fisher Scientific), starting in the nucleotide 14 of the gene N. To quantify the number of copies, a serial dilution of the plasmid in the proportion of 1:10 was performed. Commercial primers and probes for the N1 gene and RNase P (endogenous control) were used for the quantification (2019-nCov CDC EUA Kit, IDT), following the CDC's instructions.

ELISA Assay. Lung homogenate was added to RIPA buffer (radioimmunoprecipitation assay buffer: 150 mM NaCl, 1% NP-40 or Triton X-100, 0.5% sodium deoxycholate, 0.1% SDS, 50 mM Tris; pH 8.0) in a proportion of 1:1 and then centrifuged at 10,000g at 4 °C for 10 min. The supernatant was collected and stored in –70 °C until use. The sandwich ELISA method was performed to detect the concentration of cytokines and chemokines using kits from R&D Systems (DuoSet), according to the manufacturer's protocols. The following targets were evaluated: IL-6, IL-10, TNF-α, IFN-1β, CCL2, CCL3, CCL4, CXCL1, CXCL2, and CXCL10.

Lung Histopathological Process and Analyses. Five micrometer lung slices were submitted to hematoxylin and eosin staining. A total of 10 photomicrographs in 40× magnification per animal were randomly obtained using a microscope Novel (Novel L3000 LED, China) coupled to an HDI camera for image capture. The total septal area and total area were analyzed with the aid of the Pro Plus 7 software (Media Cybernetics, Inc., MD, USA). Morphometric analysis was performed in accordance with the protocol established by the American Thoracic Society and European Thoracic Society (ATS/ERS).⁷⁹

All reagents and solvents were purchased from commercial suppliers and used without further purification. ^1H and ^{13}C spectra were measured on Bruker AC-300 (300 MHz, ^1H) or Bruker AC-200 (50 MHz, ^{13}C). Chemical shifts were measured in DMSO- d_6 or CDCl_3 using tetramethylsilane as an internal standard and reported as unit (ppm) values. The following abbreviations are used to indicate the multiplicity: s, singlet; d, doublet; t, triplet; m, multiplet; dd, doublet of doublets; brs, broad singlet; and brm, broad multiplet.

The purity of the final compounds was analyzed on an Agilent 1290 Infinity II HPLC system coupled to an Agilent 6460 triple-quadrupole mass spectrometer equipped with an electrospray ionization source. The chromatographic separation was carried out on an Agilent Eclipse Plus C18 RRHD column (2.1 \times 50 mm, 1.8 μm) at 40 $^\circ\text{C}$, and the sample injection volume was 0.2 μL . The mobile phase comprising 0.1% formic acid/water (A) and 0.1% formic acid and 85% acetonitrile/water (B) was programmed with gradient elution (0.0–3.0 min, 60% B; 3.0–4.0 min, 60–97% B; 4.0–6.0 min, 97% B; 6.0–6.1 min, 97–60% B) at a flow rate of 0.4 mL/min. The mass spectrometric detection was operated in positive ion mode. Optimal parameters were capillary voltages of 3500 V, a nebulizer pressure of 35 psi, a gas temperature of 350 $^\circ\text{C}$, and a gas flow rate of 12 L/min. All final compounds are >95% pure. Melting points were determined on Electrothermal 9001 (10 $^\circ\text{C}$ per min) and are uncorrected. Merck KGaA silica gel 60 F₂₅₄ plates were used for analytical thin-layer chromatography. Column chromatography was performed on Merck silica gel 60 (70–230 mesh). Yields refer to purified products and are not optimized.

The molecules were synthesized, according to Schemes 1 or 2, and the specific methods and analytical results are described in the Supporting Information.

Molecule Synthesis. *4-[(6-Chloro-2-methoxyacridin-9-yl)amino]phenol 2 (12126037)*. Solid 2-aminophenol (0.39 g, 3.6 mmol) was added to a suspension of starting 6,9-dichloro-2-methoxyacridine 1 (0.5 g, 1.8 mmol) in 10 mL of dimethylformamide. The reaction mass was stirred at reflux for 1 h and cooled, and the precipitate was filtered off and washed with DMF, EtOH, and diethyl ether. The yield was 72%. Mp 290 $^\circ\text{C}$ with decomposition, (DMF). Mass (EI), m/z ($I_{\text{relat.}}$ (%)): 350.7981 [$\text{M}]^+$ (92). $\text{C}_{20}\text{H}_{15}\text{Cl}_2\text{N}_2\text{O}_2$. ^1H NMR (DMSO- d_6 ; δ , ppm): 9.98 (1H, s, NH), 8.16 (3H, m, 3CH), 7.73 (2H, m, 2CH), 7.47 (1H, d, $J = 4.5$, CH), 7.23 (2H, d, $J = 6.5$, 2CH), 6.92 (2H, d, $J = 6.5$, 2CH), 3.81 (3H, s, OCH_3). ^{13}C NMR (DMSO- d_6 ; δ , ppm): 156.0, 152.9, 147.8, 147.6, 145.1, 144.7, 133.7, 131.3, 131.1, 128.1, 122.8, 121.8, 121.5, 121.4, 120.9, 120.3, 120.1, 117.9, 101.0, 55.7.

4-[(6-Chloro-2-methoxyacridin-9-yl)amino]-2,6-bis-[(dimethylamino)methyl]phenol 3 (12126038). A mixture of 40% aqueous solution of dimethylamine (1.1 mL, 9.0 mmol), 1 mL of acetic acid, and 37% aqueous solution of formaldehyde (0.39 mL, 5.4 mmol) was added at once to a suspension of 4-[(6-chloro-2-methoxyacridin-9-yl)amino]phenol 2 (0.9 mmol) in 10 mL of dimethylformamide. The suspension was heated to boiling and boiled for 4 h. The reaction mixture was cooled, and an aqueous solution of NaHCO_3 (17 mmol) was added, transferred to a separatory funnel, and extracted with ethyl acetate (2 \times 30 mL). The combined organic layer was washed with water (2 \times 100 mL) and dried over sodium sulfate. The solvent was removed in vacuo, and residue oil was treated with a mixture of 20 mL of hexane and 1 mL of diethyl ether. The oil was ground and kept for 10 h at 40 $^\circ\text{C}$. The solid was

filtered off, washed with hexane, and purified by column chromatography (methanol). The yield of the aim product was 25%. Mp 148–152 $^\circ\text{C}$. Mass (EI), m/z ($I_{\text{relat.}}$ (%)): 464.9869 [$\text{M}]^+$ (88). $\text{C}_{26}\text{H}_{29}\text{ClN}_4\text{O}_2$. ^1H NMR (DMSO- d_6 ; δ , ppm): 9.98 (1H, s, NH), 8.17 (3H, m, 3CH), 7.84 (2H, m, 2CH), 7.45 (1H, d, $J = 4.5$, CH), 7.06 (2H, s, 2CH), 3.81 (3H, s, OCH_3), 3.61 (2H, s, 2 CH_2), 2.78 (12H, br s, 2 N(CH_3)₂). ^{13}C NMR (DMSO- d_6 ; δ , ppm): 157.2, 156.0, 154.5, 147.8, 145.1, 144.6, 133.7, 131.3, 131.1, 128.0, 128.1, 125.5, 122.8, 121.4, 118.6, 114.9, 112.2, 101.0, 55.8, 55.7, 44.9.

4-[(6-Chloro-2-methoxyacridin-9-yl)amino]-2-(pyrrolidin-1-ylmethyl)phenol 4 and 4-[(6-Chloro-2-methoxyacridin-9-yl)amino]-2,6-bis(pyrrolidin-1-ylmethyl)phenol 5. A mixture of pyrrolidine (0.52 mL, 6.0 mmol), 0.7 mL of acetic acid, and 37% aqueous formaldehyde solution (0.28 mL, 3.6 mmol) was added to a suspension of 4-[(6-chloro-2-methoxyacridin-9-yl)amino]phenol 2 (0.6 mmol) in 10 mL of dimethylformamide. The solution was stirred at reflux for 1 h. The reaction mixture was cooled, and an aqueous solution of NaHCO_3 (11 mmol) was added and extracted with ethyl acetate (2 \times 30 mL). The combined organic layer was washed with water (2 \times 100 mL) and dried with sodium sulfate, and the solvent was evaporated in vacuo. The resulting oil was dissolved in chloroform and applied to a chromatography column (chloroform/methanol 9:1), and product 4 was isolated. Pure methanol was used as an eluent for separation product 5.

4-[(6-Chloro-2-methoxyacridin-9-yl)amino]-2-(pyrrolidin-1-ylmethyl)phenol 4 (12126040). The yield is 5%. Mp 178–182 $^\circ\text{C}$. Mass (EI), m/z ($I_{\text{relat.}}$ (%)): 433.9298 [$\text{M}]^+$ (76). $\text{C}_{25}\text{H}_{24}\text{ClN}_3\text{O}_2$. ^1H NMR (DMSO- d_6 ; δ , ppm): 10.21 (1H, s, NH), 8.17 (3H, m, 3CH), 7.81 (2H, m, 2CH), 7.45 (1H, d, $J = 4.5$, CH), 7.06 (2H, s, 2CH), 3.83 (3H, s, OCH_3), 3.60 (2H, s, 2 CH_2), 2.5–2.7 (8H, br m, 2 N(CH_2)₂), 1.6–1.8 (8H, br m, 2(CH_2)₂). ^{13}C NMR (DMSO- d_6 ; δ , ppm): 157.7, 156.2, 154.5, 147.8, 145.1, 144.3, 133.7, 131.3, 131.1, 125.5, 122.8, 121.4, 118.7, 114.9, 111.5, 101.1, 55.7, 54.1, 52.3, 23.4.

4-[(6-Chloro-2-methoxyacridin-9-yl)amino]-2,6-bis-(pyrrolidin-1-ylmethyl)phenol 5 (12126039). The yield is 10%. Mp 145–150 $^\circ\text{C}$. Mass (EI), m/z ($I_{\text{relat.}}$ (%)): 517.0615 [$\text{M}]^+$ (79). $\text{C}_{30}\text{H}_{33}\text{ClN}_4\text{O}_2$. ^1H NMR (DMSO- d_6 ; δ , ppm): 10.04 (1H, s, NH), 8.16 (3H, m, 3CH), 7.79 (2H, m, 2CH), 7.47 (1H, d, $J = 4.5$, CH), 7.06 (1H, d, $J = 4.5$, CH), 6.93 (1H, s, CH), 3.83 (3H, s, OCH_3), 3.60 (2H, s, 2 CH_2), 2.5–2.7 (8H, br m, 2 N(CH_2)₂), 1.6–1.8 (8H, br m, 2(CH_2)₂). ^{13}C NMR (DMSO- d_6 ; δ , ppm): 156.0, 152.4, 149.3, 147.7, 145.1, 139.2, 131.2, 131.1, 128.7, 124.1, 122.8, 121.2, 120.8, 116.4, 116.1, 112.4, 101.6, 55.8, 51.9, 23.42.

6-Chloro-2-methoxyacridin-9-ol 6 (12126072). The mixture of pyrrolidine (1.0 mL, 13.0 mmol), 1.4 mL of acetic acid, and 37% aqueous formaldehyde solution (0.56 mL, 7.8 mmol) was added to a suspension of 4-[(6-chloro-2-methoxyacridin-9-yl)amino]phenol 2 (1.3 mmol) in 10 mL of ethanol. The suspension was boiled for 36 h. The reaction mixture was cooled, an aqueous solution of NaHCO_3 (2.6 mmol) was added, and the precipitate of the aim compound was filtered off. The yield is 38%. Mp 300 $^\circ\text{C}$ (DMF). Mass (EI), m/z ($I_{\text{relat.}}$ (%)): 259.0615 [$\text{M}]^+$ (79). $\text{C}_{14}\text{H}_{10}\text{ClNO}_2$. ^1H NMR (DMSO- d_6 ; δ , ppm): 8.56 (1H, d, $J = 9.0$, CH), 7.72 (H, s, CH), 7.62 (1H, d, $J = 4.5$, CH), 7.44 (1H, d, $J = 4.5$, CH), 7.27 (1H, s, CH), 7.07 (1H, d, $J = 9.0$, CH), 3.86 (3H, s, OCH_3). ^{13}C NMR (DMSO- d_6 ; δ , ppm): 157.8, 148.2, 147.9, 140.6, 138.0, 136.7, 128.7, 126.9, 125.5, 124.6, 123.3, 102.9, 55.3.

6-Chloro-2-methoxy-9-morpholin-4-ylacridine 7 (12126036). Morpholine (0.23 mL, 2.7 mmol) was added to a suspension of starting 6,9-dichloro-2-methoxyacridine 1 (0.25 g, 0.9 mmol) in 7 mL of dimethylformamide. The reaction mixture was stirred at reflux for 30 min and cooled, and the formed precipitate was filtered off and washed with dimethylformamide and acetone. The yield is 70%. Mp 208–212 °C (DMF). Mass (EI), m/z ($I_{\text{relat.}}(\%)$): 328.7926 [M]⁺ (74). C₁₈H₁₇ClN₂O₂. ¹H NMR (DMSO-*d*₆; δ , ppm): 8.56 (1H, d, $J = 9.0$, CH), 7.72 (H, s, CH), 7.62 (1H, d, $J = 4.5$, CH), 7.44 (1H, d, $J = 4.5$, CH), 7.27 (1H, s, CH), 7.07 (1H, d, $J = 9.0$, CH), 3.86 (3H, s, OCH₃). ¹³C NMR (DMSO-*d*₆; δ , ppm): 155.7, 149.8, 142.6, 134.5, 131.7, 130.9, 130.6, 127.6, 122.4, 119.7, 119.1, 114.8, 100.5, 66.8, 55.7, 50.8.

(2E)-2-Cyano-3-(dimethylamino)but-2-enamide 2. Dimethyl acetal dimethylacetamide (1 mL, 7.2 mmol) was added to a suspension of cyanoacetamide 1 (0.5 g, 6 mmol) in 15 mL of absolute alcohol. The suspension was boiled for 3 h and cooled, and the obtained precipitate was filtered off and washed with alcohol and diethyl ether. Aim product 2 was obtained with a yield of 82%. Mp 188–192 °C (isopropanol).

(2E)-3-Anilino-2-cyanobut-2-enamide 3. Aniline (0.45 mL, 5 mmol) was added to a suspension of (2E)-2-cyano-3-(dimethylamino)but-2-enamide 2 (0.3 g, 2 mmol) in acetic acid (4 mL). The suspension was boiled for 3 h and cooled, and acetic acid was removed under vacuum. The residue was treated with water, and the formed precipitate was filtered off and washed with water, isopropyl alcohol, and diethyl ether. Aim product 3 was obtained with a yield of 87%. Mp 179–182 °C (isopropanol).

A Mixture of 6-[(E)-2-(Dimethylamino)vinyl]-4-oxo-1-phenyl-1,4-dihydropyrimidine-5-carbonitrile 4 and (2Z,4E)-3-Anilino-2-cyano-5-(dimethylamino)-N-[(1E)-(dimethylamino)methylene]penta-2,4-dienamide 5. Dimethylformamide diethyl acetal (1.3 mL, 7.5 mmol) was added to a suspension of (2E)-3-anilino-2-cyanobut-2-enamide 3 (0.6 g, 3 mmol) in 5 mL of absolute ethanol. The dark red solution was boiled for 6 h. Part of the solvent was removed under vacuum until a thick suspension was obtained. The precipitate was filtered off and washed with absolute alcohol and dry diethyl ether. A mixture of compounds 4 and 5 was obtained.

4-Anilino-5-formyl-2-oxo-1,2-dihydropyridine-3-carbonitrile 6. A mixture of 6-[(E)-2-(dimethylamino)vinyl]-4-oxo-1-phenyl-1,4-dihydropyrimidine-5-carbonitrile 4 and (2Z,4E)-3-anilino-2-cyano-5-(dimethylamino)-N-[(1E)-(dimethylamino)methylene]penta-2,4-dienamide 5 (5.6 g) was dissolved in 56 mL of 90% acetic acid. A precipitate formed after 30 min, and the reaction mixture was stirred at room temperature for 20 h. The precipitate was filtered off and washed with water, ethyl alcohol, and acetone. The yield is 2.3 g of aim product 6. Mp 225–230 °C (with decomposition).

3-Chloro-2,3-dihydrobenzo[*b*]-1,6-naphthyridine-4-carbonitrile 7. The 4-anilino-5-formyl-2-oxo-1,2-dihydropyridine-3-carbonitrile 6 (2.3 g) was refluxed in phosphorus oxychloride (22 mL) for 1 h. The reaction mixture was poured onto ice and stirred for 30 min. The formed precipitate was filtered off and washed with water, ethyl alcohol, and diethyl ether. Aim product 7 was obtained in 80% yield. Mp 300–304 °C (DMF).

3-Chloro-10-oxo-5,10-dihydrobenzo[*b*]-1,6-naphthyridine-4-carbonitrile 8. To a suspension of 3-chloro-2,3-dihydrobenzo[*b*]-1,6-naphthyridine-4-carbonitrile 7 (0.44 g) in 15 mL of acetone was added *m*-chloroperbenzoic acid 55% (1.45 g) in small portions and refluxed for 9 h. The reaction

mixture was cooled, and the obtained precipitate was filtered off and washed with acetone, toluene, and acetone. The aim product 8 was obtained with a yield of 50%. Mp 305 °C.

3-Morpholin-4-ylbenzo[*b*]-1,6-naphthyridine-4-carbonitrile 9 (12126035). Morpholine (0.16 mL, 1.8 mmol) was added to a suspension of 3-chloro-2,3-dihydrobenzo[*b*]-1,6-naphthyridine-4-carbonitrile 7 (0.15 g, 0.6 mmol) in 4 mL of dry dimethylformamide. The solution was boiled for 1 h, cooled, poured into 40 mL of water, and extracted two times with 30 mL of ethyl acetate. The organic fractions were additionally washed with water two times. Ethyl acetate was removed under vacuum, ethyl alcohol was added to the dry residue, and the precipitate was filtered off and washed with diethyl ether. The aim product 9 was obtained with a yield of 78%. Mp 222–225 °C (EtOH:DMF 2:1). Mass (EI), m/z ($I_{\text{relat.}}(\%)$): 290.3194 [M]⁺ (79). C₁₇H₁₄N₄O. ¹H NMR (DMSO-*d*₆; δ , ppm): 9.46 (1H, s, CH), 9.13 (1H, s, CH), 8.16 (1H, d, $J = 6.5$, CH), 7.91 (1H, s, CH), 7.44 (1H, d, $J = 6.5$, CH), 4.16 (4H, m, O(CH₂)₂), 3.78 (4H, m, N(CH₂)₂). ¹³C NMR (DMSO-*d*₆; δ , ppm): 144.9, 143.5, 137.8, 136.4, 136.0, 133.1, 129.5, 128.4, 126.8, 126.1, 114.5, 101.4, 66.7, 53.8.

3-Morpholin-4-yl-10-oxo-5,10-dihydrobenzo[*b*]-1,6-naphthyridine-4-carbonitrile 10 (10326099). Morpholine (0.14 mL, 1.6 mmol) was added to a solution of 3-chloro-10-oxo-5,10-dihydrobenzo[*b*]-1,6-naphthyridine-4-carbonitrile 8 (0.2 g, 0.8 mmol) in 5 mL of dry dimethylformamide. The formed suspension was stirred at reflux for 1 h and cooled, and the precipitate was filtered off and washed with dimethylformamide and acetone. Mp 290 °C (DMF). The yield is 38%. Mass (EI), m/z ($I_{\text{relat.}}(\%)$): 306.3188 [M]⁺ (68). C₁₇H₁₄N₄O₂. ¹H NMR (DMSO-*d*₆; δ , ppm): 8.02 (1H, s, CH), 7.91 (1H, d, $J = 6.5$, CH), 7.59 (1H, s, CH), 7.09 (1H, d, $J = 6.5$, CH), 4.08 (4H, m, O(CH₂)₂), 3.72 (4H, m, N(CH₂)₂). ¹³C NMR (DMSO-*d*₆; δ , ppm): 182.5, 146.4, 146.1, 139.7, 139.1, 138.7, 137.0, 124.9, 122.7, 118.3, 115.4, 108.8, 94.9, 66.8, 53.7.

PL^{PRO} Cloning, Expression, Purification, and Assays. The viral cDNA template (GenBank MT126808.1) was kindly provided by Dr. Edison Durigon. Amplification of the nucleotide sequence coding for the PL^{PRO} domain (residues 1564–1879 of SARS-CoV-2) was performed by polymerase chain reaction (PCR) using forward (5'- ATTCATGGGC-GAAGTGAGGACTATTAAGGTGTTTAC-3') and reverse (5'- ATTGCTCGAGTGGTTTTATGGTTGTTGTG-TAACT-3') primers, with restriction sites for *Nco*I and *Xho*I. The PCR product was digested with *Nco*I and *Xho*I and cloned into pET28a (Novagen) in frame with a C-terminal his-tag coding sequence. *Escherichia coli* BL21 transformed with plasmids was grown in LB to an optical density (OD₆₀₀) of 0.6 at 37 °C and 200 rpm. Protein expression was induced by adding 0.5 mM IPTG and 1 mM zinc chloride and grown overnight at 18°. The cell pellet was resuspended in lysis buffer (50 mM Tris, 150 mM NaCl, 10 mM imidazole, and 1 mM DTT, pH 8.5), disrupted by sonication, and centrifuged at 12,500 rpm for 40 min at 4 °C. Protein was isolated from the lysate using 5 mL of Ni-NTA resin (Qiagen) pre-equilibrated with lysis buffer and then washed with 15 column volumes (CV) with the same buffer. The his-tagged protein was eluted 4 CV of elution buffer (lysis buffer supplemented with 250 mM imidazole) and further purified by size exclusion chromatography in a Superdex 200 10/30 (GE Healthcare) equilibrated with 20 mM Tris pH 7.4, 100 mM NaCl, and 2 mM DTT.

The PL^{Pro} inhibition assay was performed using the FRET-based fluorescent peptide substrate Abz-TLKGG↓API-KEDDPS-EDDnp, kindly provided by Dr. Maria Aparecida Juliano (Federal University of São Paulo, Brazil). The assay was standardized with an enzyme concentration of 70 nM and 27 μM fluorescent substrate in PL^{Pro} assay buffer (50 mM HEPES pH 7.5, 0.01% Triton X-100, and 5 mM DTT), at 37 °C for 30 min. Activity was measured in the plate reader system Spectramax Gemini EM (Molecular Devices), with λ_{ex} = 320 nm and λ_{em} = 420 nm, in the presence of different inhibitors and 1% DMSO.

M^{Pro} Cloning, Expression, Purification, and Assays. The M^{Pro} cloning is described elsewhere.⁸⁰ For expression, BL21 cells transformed with plasmid were grown in ZYM-5052 to an OD₆₀₀ of 0.6–0.8 at 37 °C and 200 rpm. Protein expression was induced lowering the temperature to 18 °C, and cells were then grown for 16 h and harvested by centrifugation. The cell pellet was resuspended in lysis buffer (20 mM Tris pH 7.8, 150 mM NaCl, and 1 mM DTT), disrupted by sonication, and centrifuged at 12,000g for 40 min at 4 °C. Uncleaved protein with 6× HisTag was isolated from the lysate using Ni-NTA resin (Qiagen). The flow-through (FT) was then used to purify cleaved protein with ammonium sulfate precipitation. Ammonium sulfate was added into the FT to a final concentration of 1 M, incubated on ice for 10 min, and centrifuged at 12,000g for 30 min at 4 °C. The precipitated protein was resuspended in gel filtration buffer (20 mM Tris pH 7.8, 150 mM NaCl, 1 mM EDTA, and 1 mM DTT) and purified by size-exclusion chromatography in a HiLoad 26/100 Superdex 200 column (GE Healthcare) pre-equilibrated with gel filtration buffer. Afterward, the protein was buffer-exchanged to 20 mM Tris pH 8.0 and 1.0 mM DTT, loaded into a Mono-Q 5/50 GL column (GE Healthcare) in the same buffer, and eluted with a linear gradient of a buffer containing 20 mM Tris pH 8.0, 1.0 M NaCl, and 1.0 mM DTT. Proteins were concentrated at 1.0 mg/mL, flash-frozen, and stored at –80 °C for inhibition assays.

The M^{Pro} inhibition assay was performed using the FRET-based fluorescent peptide substrate DABCYL-KTSAVLQ↓SGFRKM-E(EDANS)-NH₂ (purchased from Genscript). The assay was standardized with an enzyme concentration of 140 nM and 30 μM fluorescent substrate in M^{Pro} assay buffer containing 20 mM Tris pH 7.3, 1 mM EDTA, and 1 mM DTT, at 37 °C for 30 min. Activity was detected in the spectrofluorometer system Spectramax Gemini EM (Molecular Devices), with λ_{ex} = 360 nm and λ_{em} = 460 nm, in the presence of different inhibitors and 1% DMSO.

Kinase Profiling of Pyronaridine. Kinase profiling was performed for pyronaridine (1 μM) in duplicate by Thermo Fisher Scientific (Life Technologies Corporation, Chicago, IL 60693) using Z'Lyte,⁸¹ Adapta,⁸² and LanthaScreen⁸³ assays for 485 purified kinases.

CAMK1 Inhibition. Pyronaridine inhibition of CAMK1 was performed by Selected Services (Thermo Fisher Scientific) using the Adapta universal kinase assay, which is a homogeneous, fluorescent-based immunoassay for the detection of ADP. The 2× CAMK1 (CaMK1) and ZIPtide mixture was prepared in 50 mM HEPES pH 7.5, 0.01% BRIJ-35, 10 mM MgCl₂, 1 mM EGTA, 4 mM CaCl₂, 800 U/mL calmodulin, and 0.02% NaN₃. The final 10 μL kinase reaction consists of 0.25–1.2 ng of CAMK1 (CaMK1) and 200 μM ZIPtide in 32.5 mM HEPES pH 7.5, 0.005% BRIJ-35, 5 mM MgCl₂, 500 μM EGTA, 2 mM CaCl₂, 400 U/mL calmodulin,

and 0.01% NaN₃. After 1 h of kinase reaction incubation, 5 μL of detection mix was added.

■ ASSOCIATED CONTENT

Supporting Information

The Supporting Information is available free of charge at <https://pubs.acs.org/doi/10.1021/acsinfecdis.2c00091>.

SelectScreen kinase profiling of pyronaridine and positive control data for M^{Pro} and PL^{Pro} assays (PDF)

■ AUTHOR INFORMATION

Corresponding Authors

Ana C. Puhl – Collaborations Pharmaceuticals, Inc., Raleigh, North Carolina 27606, United States; orcid.org/0000-0002-1456-8882; Email: ana@collaborationspharma.com

Thiago M. Cunha – Center for Research in Inflammatory Diseases (CRID), Ribeirao Preto Medical School, University of São Paulo, Ribeirao Preto 14049-900 São Paulo, Brazil; Email: thicunha@fmrp.usp.br

Sean Ekins – Collaborations Pharmaceuticals, Inc., Raleigh, North Carolina 27606, United States; orcid.org/0000-0002-5691-5790; Email: sean@collaborationspharma.com

Authors

Giovanni F. Gomes – Center for Research in Inflammatory Diseases (CRID), Ribeirao Preto Medical School, University of São Paulo, Ribeirao Preto 14049-900 São Paulo, Brazil

Samara Damasceno – Center for Research in Inflammatory Diseases (CRID), Ribeirao Preto Medical School, University of São Paulo, Ribeirao Preto 14049-900 São Paulo, Brazil

Andre S. Godoy – Institute of Physics of Sao Carlos, University of São Paulo, Sao Carlos 13563-120, Brazil

Gabriela D. Noske – Institute of Physics of Sao Carlos, University of São Paulo, Sao Carlos 13563-120, Brazil

Aline M. Nakamura – Institute of Physics of Sao Carlos, University of São Paulo, Sao Carlos 13563-120, Brazil

Victor O. Gawriljuk – Institute of Physics of Sao Carlos, University of São Paulo, Sao Carlos 13563-120, Brazil

Rafaela S. Fernandes – Institute of Physics of Sao Carlos, University of São Paulo, Sao Carlos 13563-120, Brazil

Natalia Monakhova – Research Center of Biotechnology RAS, 119071 Moscow, Russia

Olga Riabova – Research Center of Biotechnology RAS, 119071 Moscow, Russia

Thomas R. Lane – Collaborations Pharmaceuticals, Inc., Raleigh, North Carolina 27606, United States

Vadim Makarov – Research Center of Biotechnology RAS, 119071 Moscow, Russia

Flavio P. Veras – Center for Research in Inflammatory Diseases (CRID), Ribeirao Preto Medical School, University of São Paulo, Ribeirao Preto 14049-900 São Paulo, Brazil

Sabrina S. Batah – Department of Pathology and Legal Medicine, Ribeirão Preto Medical School, University of São Paulo, Ribeirao Preto 14049-900 São Paulo, Brazil

Alexandre T. Fabro – Department of Pathology and Legal Medicine, Ribeirão Preto Medical School, University of São Paulo, Ribeirao Preto 14049-900 São Paulo, Brazil

Glaucius Oliva – Institute of Physics of Sao Carlos, University of São Paulo, Sao Carlos 13563-120, Brazil

Fernando Q. Cunha – Center for Research in Inflammatory Diseases (CRID), Ribeirao Preto Medical School, University of São Paulo, Ribeirao Preto 14049-900 São Paulo, Brazil

José C. Alves-Filho – Center for Research in Inflammatory Diseases (CRID), Ribeirão Preto Medical School, University of São Paulo, Ribeirão Preto 14049-900 São Paulo, Brazil

Complete contact information is available at:

<https://pubs.acs.org/10.1021/acsinfectdis.2c00091>

Author Contributions

[#]A.C.P. and G.F.G. contribute equally. A.C.P., T.M.C., and S.E. conceived and codirected the study. A.C.P., G.F.G., A.S.G., V.M., G.O., F.Q.C., J.C.A.-F., and T.M.C. designed the experiments; A.C.P., S.D., G.D.N., A.M.N., V.O.G., R.S.F., N.M., O.R., S.S.B., and A.T.F. performed *in vitro* experiments. G.F.G., S.D., and F.P.V. performed *in vivo* experiments. A.C.P., S.E., G.F.G., A.S.G., T.M.C., and T.R.L. wrote the manuscript. All authors read and accepted the manuscript.

Notes

The authors declare the following competing financial interest(s): S.E. is CEO of Collaborations Pharmaceuticals, Inc. A.C.P. and T.R.L. are employees at Collaborations Pharmaceuticals, Inc. All other authors have no competing interests.

We kindly acknowledge NIH funding: S.E. kindly acknowledges NIH funding R44GM122196-02A1 from NIH NIGMS 1R43AT010585-01 and from NIH/NCCAM, G.O. and colleagues acknowledge Coordenação de Aperfeiçoamento de Pessoal de Nível Superior (CAPES – project 88887.516153/2020-00) and Fundação de Amparo à Pesquisa do Estado de São Paulo (FAPESP project 2013/07600-3). T.M.C., J.C.A.-F., and F.Q.C. received funding from the São Paulo Research Foundation (FAPESP) under grant agreements 2013/08216-2 (Center for Research in Inflammatory Disease) and 2020/04860-8 and from Coordenação de Aperfeiçoamento de Pessoal de Nível Superior (project 88887.507155/2020-00). N.M., O.R., and V.M. acknowledge RFBR (project 20-54-80006).

This article has been submitted to BiorXiv doi: <https://doi.org/10.1101/2021.09.30.462449>.

ACKNOWLEDGMENTS

The authors would like to kindly acknowledge their many collaborators around the world who have assisted in our various COVID-19 projects. The authors gratefully acknowledge the technical assistance of Marcella Daruge Grando, Ieda Regina dos Santos, Juliana Trench Abumansur, and Felipe Souza. We kindly acknowledge Prof. Carlos Alberto Montanari (University of São Paulo, Brazil) for providing nirmatrelvir.

ABBREVIATIONS USED

ACE2, angiotensin converting enzyme 2; BMP, bis-(monoacylglycero)phosphate; COVID-19, coronavirus disease; MERS-CoV, Middle East Respiratory Syndrome coronavirus; SARS-CoV-2, severe acute respiratory coronavirus 2

REFERENCES

- (1) Wu, F.; Zhao, S.; Yu, B.; Chen, Y. M.; Wang, W.; Song, Z. G.; Hu, Y.; Tao, Z. W.; Tian, J. H.; Pei, Y. Y.; Yuan, M. L.; Zhang, Y. L.; Dai, F. H.; Liu, Y.; Wang, Q. M.; Zheng, J. J.; Xu, L.; Holmes, E. C.; Zhang, Y. Z. Author Correction: A new coronavirus associated with human respiratory disease in China. *Nature* **2020**, *580*, E7.
- (2) Coronaviridae Study Group of the International Committee on Taxonomy of Viruses. The species Severe acute respiratory syndrome-

related coronavirus: classifying 2019-nCoV and naming it SARS-CoV-2. *Nat Microbiol.* **2020**, *5*, 536–544.

(3) WHO Naming the coronavirus disease (COVID-2019) and the virus that causes it. [https://www.who.int/emergencies/diseases/novel-coronavirus-2019/technical-guidance/naming-the-coronavirus-disease-\(covid-2019\)-and-the-virus-that-causes-it](https://www.who.int/emergencies/diseases/novel-coronavirus-2019/technical-guidance/naming-the-coronavirus-disease-(covid-2019)-and-the-virus-that-causes-it).

(4) Rehman, M. F. U.; Fariha, C.; Anwar, A.; Shahzad, N.; Ahmad, M.; Mukhtar, S.; Haque, M. F. U. Novel coronavirus disease (COVID-19) pandemic: A recent mini review. *Comput. Struct. Biotechnol. J.* **2021**, *19*, 612–623.

(5) Kyriakidis, N. C.; López-Cortés, A.; González, E. V.; Grimaldos, A. B.; Prado, E. O. SARS-CoV-2 vaccines strategies: a comprehensive review of phase 3 candidates. *npj Vaccines* **2021**, *6*, 28.

(6) Huang, H. Y.; Wang, S. H.; Tang, Y.; Sheng, W.; Zuo, C. J.; Wu, D. W.; Fang, H.; Du, Q.; Li, N. Landscape and progress of global COVID-19 vaccine development. *Hum. Vaccines Immunother.* **2021**, *3276–3280*.

(7) Hall, M. D.; Anderson, J. M.; Anderson, A.; Baker, D.; Bradner, J.; Brimacombe, K. R.; Campbell, E. A.; Corbett, K. S.; Carter, K.; Cherry, S.; Chiang, L.; Cihlar, T.; de Wit, E.; Denison, M.; Disney, M.; Fletcher, C. V.; Ford-Scheimer, S. L.; Gotte, M.; Grossman, A. C.; Hayden, F. G.; Hazuda, D. J.; Lanteri, C. A.; Marston, H.; Mesecar, A. D.; Moore, S.; Nwankwo, J. O.; O’Rear, J.; Painter, G.; Singh Saikatendu, K.; Schiffer, C. A.; Sheahan, T. P.; Shi, P. Y.; Smyth, H. D.; Sofia, M. J.; Weetall, M.; Weller, S. K.; Whitley, R.; Fauci, A. S.; Austin, C. P.; Collins, F. S.; Conley, A. J.; Davis, M. I. Report of the National Institutes of Health SARS-CoV-2 Antiviral Therapeutics Summit. *J. Infect. Dis.* **2021**, *224*, S1–S21.

(8) Eastman, R. T.; Roth, J. S.; Brimacombe, K. R.; Simeonov, A.; Shen, M.; Patnaik, S.; Hall, M. D. Remdesivir: A Review of Its Discovery and Development Leading to Emergency Use Authorization for Treatment of COVID-19. *ACS Cent. Sci.* **2020**, *6*, 672–683.

(9) Wang, M.; Cao, R.; Zhang, L.; Yang, X.; Liu, J.; Xu, M.; Shi, Z.; Hu, Z.; Zhong, W.; Xiao, G. Remdesivir and chloroquine effectively inhibit the recently emerged novel coronavirus (2019-nCoV) *in vitro*. *Cell Res.* **2020**, *30*, 269–271.

(10) Pruijssers, A. J.; George, A. S.; Schafer, A.; Leist, S. R.; Gralinski, L. E.; Dinnon, K. H., III; Yount, B. L.; Agostini, M. L.; Stevens, L. J.; Chappell, J. D.; Lu, X.; Hughes, T. M.; Gully, K.; Martinez, D. R.; Brown, A. J.; Graham, R. L.; Perry, J. K.; Du Pont, V.; Pitts, J.; Ma, B.; Babusis, D.; Murakami, E.; Feng, J. Y.; Bilello, J. P.; Porter, D. P.; Cihlar, T.; Baric, R. S.; Denison, M. R.; Sheahan, T. P. Remdesivir Inhibits SARS-CoV-2 in Human Lung Cells and Chimeric SARS-CoV Expressing the SARS-CoV-2 RNA Polymerase in Mice. *Cell Rep.* **2020**, *32*, No. 107940.

(11) Mulangu, S.; Dodd, L. E.; Davey, R. T., Jr.; Tshiani Mbaya, O.; Proschan, M.; Mukadi, D.; Lusakibanza Manzo, M.; Nzolo, D.; Tshomba Oloma, A.; Ibanda, A.; Ali, R.; Coulibaly, S.; Levine, A. C.; Grais, R.; Diaz, J.; Lane, H. C.; Muyembe-Tamfum, J. J.; Group, P. W.; Sivahera, B.; Camara, M.; Kojan, R.; Walker, R.; Dighero-Kemp, B.; Cao, H.; Mukumbayi, P.; Mbala-Kingebeni, P.; Ahuka, S.; Albert, S.; Bonnett, T.; Crozier, I.; Duvenhage, M.; Proffitt, C.; Teitelbaum, M.; Moench, T.; Aboulhab, J.; Barrett, K.; Cahill, K.; Cone, K.; Eckes, R.; Hensley, L.; Herpin, B.; Higgs, E.; Ledgerwood, J.; Pierson, J.; Smolskis, M.; Sow, Y.; Tierney, J.; Sivapalasingam, S.; Holman, W.; Gettinger, N.; Vallee, D.; Nordwall, J.; Team, P. C. S. A Randomized, Controlled Trial of Ebola Virus Disease Therapeutics. *N Engl. J. Med.* **2019**, *381*, 2293–2303.

(12) Ekins, S.; Freundlich, J. S.; Clark, A. M.; Anantpadma, M.; Davey, R. A.; Madrid, P. Machine learning models identify molecules active against Ebola virus *in vitro*. *PLoS One* **2015**, *4*, 1091.

(13) Lane, T. R.; Massey, C.; Comer, J. E.; Anantpadma, M.; Freundlich, J. S.; Davey, R. A.; Madrid, P. B.; Ekins, S. Repurposing the antimalarial pyronaridine tetraphosphate to protect against Ebola virus infection. *PLoS Neglected Trop. Dis.* **2019**, *13*, No. e0007890.

(14) Lane, T. R.; Comer, J. E.; Freiberg, A. N.; Madrid, P. B.; Ekins, S. Repurposing Quinacrine Against Ebola Virus Infection *In vivo*. *Antimicrob. Agents Chemother.* **2019**, *63*, e011142–e011119.

- (15) Ekins, S.; Lingerfelt, M. A.; Comer, J. E.; Freiberg, A. N.; Mirsalis, J. C.; O'Loughlin, K.; Harutyunyan, A.; McFarlane, C.; Green, C. E.; Madrid, P. B. Efficacy of Tilorone Dihydrochloride against Ebola Virus Infection. *Antimicrob. Agents Chemother.* **2018**, *62*, No. e01711-17.
- (16) Lane, T. R.; Ekins, S. Towards the Target: Tilorone, Quinacrine and Pyronaridine Bind to Ebola Virus Glycoprotein. *ACS Med. Chem. Lett.* **2020**, *11*, 1653–1658.
- (17) Lane, T. R.; Massey, C.; Comer, J. E.; Freiberg, A. N.; Zhou, H.; Dyall, J.; Holbrook, M. R.; Anantpadma, M.; Davey, R. A.; Madrid, P. B.; Ekins, S. Efficacy of Oral Pyronaridine Tetraphosphate and Favipiravir Against Ebola Virus Infection in Guinea Pig. *Antiviral Res.* **2020**, *181*, No. 104863.
- (18) Puhl, A. C.; Fritch, E. J.; Lane, T. R.; Tse, L. V.; Yount, B. L.; Sacramento, C. Q.; Fintelman-Rodrigues, N.; Tavella, T. A.; Maranhao Costa, F. T.; Weston, S.; Logue, J.; Frieman, M.; Premkumar, L.; Pearce, K. H.; Hurst, B. L.; Andrade, C. H.; Levi, J. A.; Johnson, N. J.; Kisthardt, S. C.; Scholle, F.; Souza, T. M. L.; Moorman, N. J.; Baric, R. S.; Madrid, P. B.; Ekins, S. Repurposing the Ebola and Marburg Virus Inhibitors Tilorone, Quinacrine, and Pyronaridine: In Vitro Activity against SARS-CoV-2 and Potential Mechanisms. *ACS Omega* **2021**, *6*, 7454–7468.
- (19) Jeon, S.; Ko, M.; Lee, J.; Choi, I.; Byun, S. Y.; Park, S.; Shum, D.; Kim, S. Identification of antiviral drug candidates against SARS-CoV-2 from FDA-approved drugs. *Antimicrob. Agents Chemother.* **2020**, *64*, e00819–e00820.
- (20) Bae, J.-Y.; Lee, G. E.; Park, H.; Cho, J.; Kim, Y.-E.; Lee, J.-Y.; Ju, C.; Kim, W.-K.; Kim, J. I.; Park, M.-S. Pyronaridine and artesunate are potential antiviral drugs against COVID-19 and influenza. *bioRxiv* **2020**, DOI: 10.1101/2020.07.28.225102.
- (21) Aherfi, S.; Pradines, B.; Devaux, C.; Honore, S.; Colson, P.; Scola, B.; Raoult, D. Drug repurposing against SARS-CoV-1, SARS-CoV-2 and MERS-CoV. *Future Microbiol.* **2021**, *16*, 1341–1370.
- (22) McCray, P. B., Jr.; Pewe, L.; Wohlford-Lenane, C.; Hickey, M.; Manzel, L.; Shi, L.; Netland, J.; Jia, H. P.; Halabi, C.; Sigmund, C. D.; Meyerholz, D. K.; Kirby, P.; Look, D. C.; Perlman, S. Lethal infection of K18-hACE2 mice infected with severe acute respiratory syndrome coronavirus. *J. Virol.* **2007**, *81*, 813–821.
- (23) Oladunni, F. S.; Park, J. G.; Pino, P. A.; Gonzalez, O.; Akhter, A.; Allué-Guardia, A.; Olmo-Fontán, A.; Gautam, S.; Garcia-Vilanova, A.; Ye, C.; Chiem, K.; Headley, C.; Dwivedi, V.; Parodi, L. M.; Alfson, K. J.; Staples, H. M.; Schami, A.; Garcia, J. I.; Whigham, A.; Platt, R. N., 2nd; Gazi, M.; Martinez, J.; Chuba, C.; Earley, S.; Rodriguez, O. H.; Mdaki, S. D.; Kavelish, K. N.; Escalona, R.; Hallam, C. R. A.; Christie, C.; Patterson, J. L.; Anderson, T. J. C.; Carrion, R., Jr.; Dick, E. J., Jr.; Hall-Urson, S.; Schlesinger, L. S.; Alvarez, X.; Kaushal, D.; Giavedoni, L. D.; Turner, J.; Martinez-Sobrido, L.; Torrelles, J. B. Lethality of SARS-CoV-2 infection in K18 human angiotensin-converting enzyme 2 transgenic mice. *Nat. Commun.* **2020**, *11*, 6122.
- (24) Bao, L.; Deng, W.; Huang, B.; Gao, H.; Liu, J.; Ren, L.; Wei, Q.; Yu, P.; Xu, Y.; Qi, F.; Qu, Y.; Li, F.; Lv, Q.; Wang, W.; Xue, J.; Gong, S.; Liu, M.; Wang, G.; Wang, S.; Song, Z.; Zhao, L.; Liu, P.; Zhao, L.; Ye, F.; Wang, H.; Zhou, W.; Zhu, N.; Zhen, W.; Yu, H.; Zhang, X.; Guo, L.; Chen, L.; Wang, C.; Wang, Y.; Wang, X.; Xiao, Y.; Sun, Q.; Liu, H.; Zhu, F.; Ma, C.; Yan, L.; Yang, M.; Han, J.; Xu, W.; Tan, W.; Peng, X.; Jin, Q.; Wu, G.; Qin, C. The pathogenicity of SARS-CoV-2 in hACE2 transgenic mice. *Nature* **2020**, *583*, 830–833.
- (25) Zheng, J.; Wong, L.-Y. R.; Li, K.; Verma, A. K.; Ortiz, M. E.; Wohlford-Lenane, C.; Leidinger, M. R.; Knudson, C. M.; Meyerholz, D. K.; McCray, P. B., Jr.; Perlman, S. COVID-19 treatments and pathogenesis including anosmia in K18-hACE2 mice. *Nature* **2021**, *589*, 603–607.
- (26) Kumari, P.; Rothan, H. A.; Natekar, J. P.; Stone, S.; Pathak, H.; Strate, P. G.; Arora, K.; Brinton, M. A.; Kumar, M. Neuroinvasion and Encephalitis Following Intranasal Inoculation of SARS-CoV-2 in K18-hACE2 Mice. *Viruses* **2021**, *13*, 132.
- (27) Huang, C.; Wang, Y.; Li, X.; Ren, L.; Zhao, J.; Hu, Y.; Zhang, L.; Fan, G.; Xu, J.; Gu, X.; Cheng, Z.; Yu, T.; Xia, J.; Wei, Y.; Wu, W.; Xie, X.; Yin, W.; Li, H.; Liu, M.; Xiao, Y.; Gao, H.; Guo, L.; Xie, J.; Wang, G.; Jiang, R.; Gao, Z.; Jin, Q.; Wang, J.; Cao, B. Clinical features of patients infected with 2019 novel coronavirus in Wuhan. *Lancet* **2020**, *395*, 497–506.
- (28) Herold, T.; Jurinovic, V.; Arnreich, C.; Lipworth, B. J.; Hellmuth, J. C.; von Bergwelt-Baildon, M.; Klein, M.; Weinberger, T. Elevated levels of IL-6 and CRP predict the need for mechanical ventilation in COVID-19. *J. Allergy Clin. Immunol.* **2020**, *146*, 128–136.e4.
- (29) Wang, J.; Yang, X.; Li, Y.; Huang, J. A.; Jiang, J.; Su, N. Specific cytokines in the inflammatory cytokine storm of patients with COVID-19-associated acute respiratory distress syndrome and extrapulmonary multiple-organ dysfunction. *Virology* **2021**, *18*, 117.
- (30) Zhang, Q.; Bastard, P.; Liu, Z.; Le Pen, J.; Moncada-Velez, M.; Chen, J.; Ogishi, M.; Sabli, I. K. D.; Hodeib, S.; Korol, C.; Rosain, J.; Bilguvar, K.; Ye, J.; Bolze, A.; Bigio, B.; Yang, R.; Arias, A. A.; Zhou, Q.; Zhang, Y.; Onodi, F.; Korniotis, S.; Karpf, L.; Philippot, Q.; Chbihi, M.; Bonnet-Madin, L.; Dorgham, K.; Smith, N.; Schneider, W. M.; Razooky, B. S.; Hoffmann, H. H.; Michailidis, E.; Moens, L.; Han, J. E.; Lorenzo, L.; Bizien, L.; Meade, P.; Neehus, A. L.; Ugurbil, A. C.; Corneau, A.; Kerner, G.; Zhang, P.; Rapaport, F.; Seeleuthner, Y.; Manry, J.; Masson, C.; Schmitt, Y.; Schlüter, A.; Le Voyer, T.; Khan, T.; Li, J.; Fellay, J.; Roussel, L.; Shahrooei, M.; Alosaimi, M. F.; Mansouri, D.; Al-Saud, H.; Al-Mulla, F.; Almourfi, F.; Al-Muhsen, S. Z.; Alshome, F.; Al Turki, S.; Hasanato, R.; van de Beek, D.; Biondi, A.; Bettini, L. R.; D'Angio, M.; Bonfanti, P.; Imberti, L.; Sottini, A.; Paghera, S.; Quiros-Roldan, E.; Rossi, C.; Oler, A. J.; Tompkins, M. F.; Alba, C.; Vandernoot, I.; Goffard, J. C.; Smits, G.; Migeotte, I.; Haerynck, F.; Soler-Palacin, P.; Martin-Nalda, A.; Colobran, R.; Morange, P. E.; Keles, S.; Çölkesen, F.; Özcelik, T.; Yasar, K. K.; Senoglu, S.; Karabela, Ş.; Rodríguez-Gallego, C.; Novelli, G.; Hraiech, S.; Tandjaoui-Lambiotte, Y.; Duval, X.; Laouénan, C.; Snow, A. L.; Dalgard, C. L.; Milner, J. D.; Vinh, D. C.; Mogensen, T. H.; Marr, N.; Spaan, A. N.; Boisson, B.; Boisson-Dupuis, S.; Bustamante, J.; Puel, A.; Ciancanelli, M. J.; Meyts, I.; Maniatis, T.; Soumelis, V.; Amara, A.; Nussenzeig, M.; García-Sastre, A.; Kramer, F.; Pujol, A.; Duffy, D.; Lifton, R. P.; Zhang, S. Y.; Gorochov, G.; Béziat, V.; Jouanguy, E.; Sancho-Shimizu, V.; Rice, C. M.; Abel, L.; Notarangelo, L. D.; Cobat, A.; Su, H. C.; Casanova, J. L. Inborn errors of type I IFN immunity in patients with life-threatening COVID-19. *Science* **2020**, *370*, No. eabd4570.
- (31) Xia, H.; Cao, Z.; Xie, X.; Zhang, X.; Chen, J. Y.; Wang, H.; Menachery, V. D.; Rajsbaum, R.; Shi, P. Y. Evasion of Type I Interferon by SARS-CoV-2. *Cell Rep.* **2020**, *33*, No. 108234.
- (32) Yuen, C.-K.; Lam, J.-Y.; Wong, W.-M.; Mak, L.-F.; Wang, X.; Chu, H.; Cai, J.-P.; Jin, D.-Y.; To, K. K.-W.; Chan, J. F.-W.; Yuen, K.-Y.; Kok, K.-H. SARS-CoV-2 nsp13, nsp14, nsp15 and orf6 function as potent interferon antagonists. *Emerging Microbes Infect.* **2020**, *9*, 1418–1428.
- (33) Molony, R. D.; Nguyen, J. T.; Kong, Y.; Montgomery, R. R.; Shaw, A. C.; Iwasaki, A. Aging impairs both primary and secondary RIG-I signaling for interferon induction in human monocytes. *Sci. Signaling* **2017**, *10*, No. eaan2392.
- (34) Hu, R.; Xia, C. Q.; Butfiloski, E.; Clare-Salzler, M. Effect of high glucose on cytokine production by human peripheral blood immune cells and type I interferon signaling in monocytes: Implications for the role of hyperglycemia in the diabetes inflammatory process and host defense against infection. *Clin. Immunol.* **2018**, *195*, 139–148.
- (35) Hadjadj, J.; Yatim, N.; Barnabei, L.; Corneau, A.; Boussier, J.; Smith, N.; Pere, H.; Charbit, B.; Bondet, V.; Chenevier-Gobeaux, C.; Breillat, P.; Carlier, N.; Gauzit, R.; Morbieu, C.; Pene, F.; Marin, N.; Roche, N.; Szwebel, T. A.; Merklings, S. H.; Treluyer, J. M.; Veyer, D.; Mouthon, L.; Blanc, C.; Tharaux, P. L.; Rozenberg, F.; Fischer, A.; Duffy, D.; Rieux-Laucat, F.; Kerneis, S.; Terrier, B. Impaired type I interferon activity and inflammatory responses in severe COVID-19 patients. *Science* **2020**, *369*, 718–724.
- (36) Teijaro, J. R. Type I interferons in viral control and immune regulation. *Curr. Opin. Virol.* **2016**, *16*, 31–40.

- (37) McNab, F.; Mayer-Barber, K.; Sher, A.; Wack, A.; O'Garra, A. Type I interferons in infectious disease. *Nat. Rev. Immunol.* **2015**, *15*, 87–103.
- (38) Katze, M. G.; He, Y.; Gale, M., Jr. Viruses and interferon: a fight for supremacy. *Nat. Rev. Immunol.* **2002**, *2*, 675–687.
- (39) Lee, J. S.; Shin, E. C. The type I interferon response in COVID-19: implications for treatment. *Nat. Rev. Immunol.* **2020**, *20*, 585–586.
- (40) Caramaschi, S.; Kapp, M. E.; Miller, S. E.; Eisenberg, R.; Johnson, J.; Epperly, G.; Maiorana, A.; Silvestri, G.; Giannico, G. A. Histopathological findings and clinicopathologic correlation in COVID-19: a systematic review. *Mod. Pathol.* **2021**, *34*, 1614–1633.
- (41) Pannone, G.; Caponio, V. C. A.; De Stefano, I. S.; Ramunno, M. A.; Meccariello, M.; Agostinone, A.; Pedicillo, M. C.; Troiano, G.; Zhurakivska, K.; Cassano, T.; Bizzoca, M. E.; Papagerakis, S.; Buonaguro, F. M.; Advani, S.; Muzio, L. L. Lung histopathological findings in COVID-19 disease - a systematic review. *Infect. Agents Cancer* **2021**, *16*, 34.
- (42) Hariri, L. P.; North, C. M.; Shih, A. R.; Israel, R. A.; Maley, J. H.; Villalba, J. A.; Vinarsky, V.; Rubin, J.; Okin, D. A.; Sclafani, A.; Alladina, J. W.; Griffith, J. W.; Gillette, M. A.; Raz, Y.; Richards, C. J.; Wong, A. K.; Ly, A.; Hung, Y. P.; Chivukula, R. R.; Petri, C. R.; Calhoun, T. F.; Brenner, L. N.; Hibbert, K. A.; Medoff, B. D.; Hardin, C. C.; Stone, J. R.; Mino-Kenudson, M. Lung Histopathology in Coronavirus Disease 2019 as Compared With Severe Acute Respiratory Syndrome and H1N1 Influenza: A Systematic Review. *Chest* **2021**, *159*, 73–84.
- (43) Jin, Z.; Du, X.; Xu, Y.; Deng, Y.; Liu, M.; Zhao, Y.; Zhang, B.; Li, X.; Zhang, L.; Peng, C.; Duan, Y.; Yu, J.; Wang, L.; Yang, K.; Liu, F.; Jiang, R.; Yang, X.; You, T.; Liu, X.; Bai, F.; Liu, H.; Guddat, L. W.; Xu, W.; Xiao, G.; Qin, C.; Shi, Z.; Jiang, H.; Rao, Z.; Yang, H. Structure of M^{pro} from SARS-CoV-2 and discovery of its inhibitors. *Nature* **2020**, *582*, 289–293.
- (44) Shin, D.; Mukherjee, R.; Grewe, D.; Bojkova, D.; Baek, K.; Bhattacharya, A.; Schulz, L.; Widera, M.; Mehdipour, A. R.; Tascher, G.; Geurink, P. P.; Wilhelm, A.; van der Heden van Noort, G. J.; Ova, H.; Müller, S.; Knobloch, K. P.; Rajalingam, K.; Schulman, B. A.; Cinatl, J.; Hummer, G.; Ciesek, S.; Dikic, I. Papain-like protease regulates SARS-CoV-2 viral spread and innate immunity. *Nature* **2020**, *587*, 657–662.
- (45) Qiao, J.; Li, Y. S.; Zeng, R.; Liu, F. L.; Luo, R. H.; Huang, C.; Wang, Y. F.; Zhang, J.; Quan, B.; Shen, C.; Mao, X.; Liu, X.; Sun, W.; Yang, W.; Ni, X.; Wang, K.; Xu, L.; Duan, Z. L.; Zou, Q. C.; Zhang, H. L.; Qu, W.; Long, Y. H.; Li, M. H.; Yang, R. C.; You, J.; Zhou, Y.; Yao, R.; Li, W. P.; Liu, J. M.; Chen, P.; Liu, Y.; Lin, G. F.; Yang, X.; Zou, J.; Li, L.; Hu, Y.; Lu, G. W.; Li, W. M.; Wei, Y. Q.; Zheng, Y. T.; Lei, J.; Yang, S. SARS-CoV-2 M. *Science* **2021**, *371*, 1374–1378.
- (46) Owen, D. R.; Allerton, C. M. N.; Anderson, A. S.; Aschenbrenner, L.; Avery, M.; Berritt, S.; Boras, B.; Cardin, R. D.; Carlo, A.; Coffman, K. J.; Dantonio, A.; Di, L.; Eng, H.; Ferre, R.; Gajiwala, K. S.; Gibson, S. A.; Greasley, S. E.; Hurst, B. L.; Kadar, E. P.; Kalgutkar, A. S.; Lee, J. C.; Lee, J.; Liu, W.; Mason, S. W.; Noell, S.; Novak, J. J.; Obach, R. S.; Ogilvie, K.; Patel, N. C.; Pettersson, M.; Rai, D. K.; Reese, M. R.; Sammons, M. F.; Sathish, J. G.; Singh, R. S. P.; Stepan, C. M.; Stewart, A. E.; Tuttle, J. B.; Updyke, L.; Verhoest, P. R.; Wei, L.; Yang, Q.; Zhu, Y. An oral SARS-CoV-2 M^{pro} inhibitor clinical candidate for the treatment of COVID-19. *Science* **2021**, *1586*–1593.
- (47) Ghosh, A. K.; Takayama, J.; Rao, K. V.; Ratia, K.; Chaudhuri, R.; Mulhearn, D. C.; Lee, H.; Nichols, D. B.; Baliji, S.; Baker, S. C.; Johnson, M. E.; Mesecar, A. D. Severe Acute Respiratory Syndrome Coronavirus Papain-like Novel Protease Inhibitors: Design, Synthesis, Protein–Ligand X-ray Structure and Biological Evaluation. *J. Med. Chem.* **2010**, *53*, 4968–4979.
- (48) Fu, Z.; Huang, B.; Tang, J.; Liu, S.; Liu, M.; Ye, Y.; Liu, Z.; Xiong, Y.; Zhu, W.; Cao, D.; Li, J.; Niu, X.; Zhou, H.; Zhao, Y. J.; Zhang, G.; Huang, H. The complex structure of GRL0617 and SARS-CoV-2 PLpro reveals a hot spot for antiviral drug discovery. *Nat. Commun.* **2021**, *12*, 488.
- (49) Narayanan, A.; Narwal, M.; Majowicz, S. A.; Varricchio, C.; Toner, S. A.; Ballatore, C.; Brancale, A.; Murakami, K. S.; Jose, J. Identification of SARS-CoV-2 inhibitors targeting Mpro and PLpro using in-cell-protease assay. *Commun. Biol.* **2022**, *5*, 169.
- (50) Shen, Z.; Ratia, K.; Cooper, L.; Kong, D.; Lee, H.; Kwon, Y.; Li, Y.; Alqarni, S.; Huang, F.; Dubrovskiy, O.; Rong, L.; Thatcher, G. R. J.; Xiong, R. Design of SARS-CoV-2 PLpro Inhibitors for COVID-19 Antiviral Therapy Leveraging Binding Cooperativity. *J. Med. Chem.* **2022**, *65*, 2940–2955.
- (51) Costela-Ruiz, V. J.; Illescas-Montes, R.; Puerta-Puerta, J. M.; Ruiz, C.; Melguizo-Rodríguez, L. SARS-CoV-2 infection: The role of cytokines in COVID-19 disease. *Cytokine Growth Factor Rev.* **2020**, *54*, 62–75.
- (52) Chen, R.; Lan, Z.; Ye, J.; Pang, L.; Liu, Y.; Wu, W.; Qin, X.; Guo, Y.; Zhang, P. Cytokine Storm: The Primary Determinant for the Pathophysiological Evolution of COVID-19 Deterioration. *Front. Immunol.* **2021**, *12*, No. 589095.
- (53) Felsenstein, S.; Herbert, J. A.; McNamara, P. S.; Hedrich, C. M. COVID-19: Immunology and treatment options. *Clin. Immunol.* **2020**, *215*, No. 108448.
- (54) Peter, A. E.; Sandeep, B. V.; Rao, B. G.; Kalpana, V. L. Calming the Storm: Natural Immunosuppressants as Adjuvants to Target the Cytokine Storm in COVID-19. *Front. Pharmacol.* **2021**, *11*, No. 583777.
- (55) Roshanravan, N.; Seif, F.; Ostadrahimi, A.; Pouraghaei, M.; Ghaffari, S. Targeting Cytokine Storm to Manage Patients with COVID-19: A Mini-Review. *Arch. Med. Res.* **2020**, *51*, 608–612.
- (56) Moradian, N.; Gouravani, M.; Salehi, M. A.; Heidari, A.; Shafeghat, M.; Hamblin, M. R.; Rezaei, N. Cytokine release syndrome: inhibition of pro-inflammatory cytokines as a solution for reducing COVID-19 mortality. *Eur. Cytokine Network* **2020**, *31*, 81–93.
- (57) Beerli, C.; Yakimovich, A.; Kilcher, S.; Reynoso, G. V.; Fläschner, G.; Müller, D. J.; Hickman, H. D.; Mercer, J. Vaccinia virus hijacks EGFR signalling to enhance virus spread through rapid and directed infected cell motility. *Nat. Microbiol.* **2019**, *4*, 216–225.
- (58) Pleschka, S.; Wolff, T.; Ehrhardt, C.; Hobom, G.; Planz, O.; Rapp, U. R.; Ludwig, S. Influenza virus propagation is impaired by inhibition of the Raf/MEK/ERK signalling cascade. *Nat. Cell Biol.* **2001**, *3*, 301–305.
- (59) Paul, S. M.; Mytelka, D. S.; Dunwiddie, C. T.; Persinger, C. C.; Munos, B. H.; Lindborg, S. R.; Schacht, A. L. How to improve R&D productivity: the pharmaceutical industry's grand challenge. *Nat. Rev. Drug Discovery* **2010**, *9*, 203–214.
- (60) Muratov, E. N.; Amaro, R.; Andrade, C. H.; Brown, N.; Ekins, S.; Fourches, D.; Isayev, O.; Kozakov, D.; Medina-Franco, J. L.; Merz, K. M.; Oprea, T. I.; Poroikov, V.; Schneider, G.; Todd, M. H.; Varnek, A.; Winkler, D. A.; Zakharov, A. V.; Cherkasov, A.; Tropsha, A. A critical overview of computational approaches employed for COVID-19 drug discovery. *Chem. Soc. Rev.* **2021**, *50*, 9121–9151.
- (61) Tummino, T. A.; Rezelj, V. V.; Fischer, B.; Fischer, A.; O'Meara, M. J.; Monel, B.; Vallet, T.; White, K. M.; Zhang, Z.; Alon, A.; Schadt, H.; O'Donnell, H. R.; Lyu, J.; Rosales, R.; McGovern, B. L.; Rathnasinghe, R.; Jangra, S.; Schotsaert, M.; Galarneau, J.-R.; Krogan, N. J.; Urban, L.; Shokat, K. M.; Kruse, A. C.; García-Sastre, A.; Schwartz, O.; Moretti, F.; Vignuzzi, M.; Pognan, F.; Shoichet, B. K. Drug-induced phospholipidosis confounds drug repurposing for SARS-CoV-2. *Science* **2021**, *373*, 541–547.
- (62) Lane, T. R.; Ekins, S. Defending Antiviral Cationic Amphiphilic Drugs That May Cause Drug-Induced Phospholipidosis. *J. Chem. Inf. Model.* **2021**, *4125*.
- (63) Lane, T. R.; Dyall, J.; Mercer, L.; Goodin, C.; Foil, D. H.; Zhou, H.; Postnikova, E.; Liang, J. Y.; Holbrook, M. R.; Madrid, P. B.; Ekins, S. Repurposing Pyramax® for the Treatment of Ebola Virus Disease: Additivity of the Lysosomotropic Pyronaridine and Non-Lysosomotropic Artesunate. *Antiviral Res.* **2020**, *182*, 104908.
- (64) Jayaraman, S. D.; Ismail, S.; Nair, N. K.; Navaratnam, V. Determination of pyronaridine in blood plasma by high-performance

liquid chromatography for application in clinical pharmacological studies. *J. Chromatogr. B: Biomed. Sci. Appl.* **1997**, *690*, 253–257.

(65) Ramanathan, S.; Karupiah, S.; Nair, N. K.; Olliaro, P. L.; Navaratnam, V.; Wernsdorfer, W. H.; Mansor, S. M. A new and simple solid-phase extraction method for LC determination of pyronaridine in human plasma. *J. Chromatogr. B* **2005**, *824*, 45–50.

(66) Croft, S. L.; Duparc, S.; Arbe-Barnes, S. J.; Craft, J. C.; Shin, C. S.; Fleckenstein, L.; Borghini-Fuhrer, I.; Rim, H. J. Review of pyronaridine anti-malarial properties and product characteristics. *Malar J* **2012**, *11*, 270.

(67) Bouchard, M. J.; Puro, R. J.; Wang, L.; Schneider, R. J. Activation and inhibition of cellular calcium and tyrosine kinase signaling pathways identify targets of the HBx protein involved in hepatitis B virus replication. *J. Virol.* **2003**, *77*, 7713–7719.

(68) Bouchard, M. J.; Wang, L. H.; Schneider, R. J. Calcium signaling by HBx protein in hepatitis B virus DNA replication. *Science* **2001**, *294*, 2376–2378.

(69) Liu, J. F.; Zhou, Y. N.; Lu, S. Y.; Yang, Y. H.; Wu, S. F.; Liu, D. P.; Peng, X. Z.; Yang, J. T. Proteomic and phosphoproteomic profiling of COVID-19-associated lung and liver injury: a report based on rhesus macaques. *Signal Transduction Targeted Ther.* **2022**, *7*, 27.

(70) Bouhaddou, M.; Memon, D.; Meyer, B.; White, K. M.; Rezelj, V. V.; Correa Marrero, M.; Polacco, B. J.; Melnyk, J. E.; Ulferts, S.; Kaake, R. M.; Batra, J.; Richards, A. L.; Stevenson, E.; Gordon, D. E.; Rojic, A.; Obernier, K.; Fabius, J. M.; Soucheray, M.; Miorin, L.; Moreno, E.; Koh, C.; Tran, Q. D.; Hardy, A.; Robinot, R.; Vallet, T.; Nilsson-Payant, B. E.; Hernandez-Armenta, C.; Dunham, A.; Weigang, S.; Knerr, J.; Modak, M.; Quintero, D.; Zhou, Y.; Dugourd, A.; Valdeolivas, A.; Patil, T.; Li, Q.; Hüttenhain, R.; Cakir, M.; Muralidharan, M.; Kim, M.; Jang, G.; Tutuncuoglu, B.; Hiatt, J.; Guo, J. Z.; Xu, J.; Bouhaddou, S.; Mathy, C. J. P.; Gaulton, A.; Manners, E. J.; Félix, E.; Shi, Y.; Goff, M.; Lim, J. K.; McBride, T.; O'Neal, M. C.; Cai, Y.; Chang, J. C. J.; Broadhurst, D. J.; Klippsten, S.; De Wit, E.; Leach, A. R.; Kortemme, T.; Shoichet, B.; Ott, M.; Saez-Rodriguez, J.; tenOever, B. R.; Mullins, R. D.; Fischer, E. R.; Kochs, G.; Grosse, R.; García-Sastre, A.; Vignuzzi, M.; Johnson, J. R.; Shokat, K. M.; Swaney, D. L.; Beltrao, P.; Krogan, N. J. The Global Phosphorylation Landscape of SARS-CoV-2 Infection. *Cell* **2020**, *182*, 685–712.e19.

(71) Anon Shin Poong reports data of antimalarial drug in Phase II Covid-19 trial. <https://www.pharmaceutical-technology.com/news/shin-poong-antimalarial-drug/>.

(72) Lind, K. F.; Østerud, B.; Hansen, E.; Jorgensen, T. Ø.; Andersen, J. H. The immunomodulatory effects of baretin and involvement of the kinases CAMK1alpha and RIPK2. *Immunopharmacol. Immunotoxicol.* **2015**, *37*, 458–464.

(73) Fromont, C.; Atzori, A.; Kaur, D.; Hashmi, L.; Greco, G.; Cabanillas, A.; Nguyen, H. V.; Jones, D. H.; Garzon, M.; Varela, A.; Stevenson, B.; Iacobini, G. P.; Lenoir, M.; Rajesh, S.; Box, C.; Kumar, J.; Grant, P.; Novitskaya, V.; Morgan, J.; Sorrell, F. J.; Redondo, C.; Kramer, A.; Harris, C. J.; Leighton, B.; Vickers, S. P.; Cheetham, S. C.; Kenyon, C.; Grabowska, A. M.; Overduin, M.; Berditchevski, F.; Weston, C. J.; Knapp, S.; Fischer, P. M.; Butterworth, S. Discovery of Highly Selective Inhibitors of Calmodulin-Dependent Kinases That Restore Insulin Sensitivity in the Diet-Induced Obesity in Vivo Mouse Model. *J. Med. Chem.* **2020**, *63*, 6784–6801.

(74) Zhang, X.; Guo, L.; Collage, R. D.; Stripay, J. L.; Tsung, A.; Lee, J. S.; Rosengart, M. R. Calcium/calmodulin-dependent protein kinase (CaMK) Ialpha mediates the macrophage inflammatory response to sepsis. *J. Leukocyte Biol.* **2011**, *90*, 249–261.

(75) Yinda, C. K.; Port, J. R.; Bushmaker, T.; Offei Owusu, I.; Purushotham, J. N.; Avanzato, V. A.; Fischer, R. J.; Schulz, J. E.; Holbrook, M. G.; Hebnner, M. J.; Rosenke, R.; Thomas, T.; Marzi, A.; Best, S. M.; de Wit, E.; Shaia, C.; van Doremalen, N.; Munster, V. J. K18-hACE2 mice develop respiratory disease resembling severe COVID-19. *PLoS Pathog.* **2021**, *17*, No. e1009195.

(76) Arce, V. M.; Costoya, J. A. SARS-CoV-2 infection in K18-ACE2 transgenic mice replicates human pulmonary disease in COVID-19. *Cell Mol. Immunol.* **2021**, *18*, 513–514.

(77) Moreau, G. B.; Burgess, S. L.; Sturek, J. M.; Donlan, A. N.; Petri, W. A., Jr.; Mann, B. J. Evaluation of K18-hACE2 Mice as a Model of SARS-CoV-2 Infection. *Am. J. Trop. Med. Hyg.* **2020**, *103*, 1215–1219.

(78) Winkler, E. S.; Bailey, A. L.; Kafai, N. M.; Nair, S.; McCune, B. T.; Yu, J.; Fox, J. M.; Chen, R. E.; Earnest, J. T.; Keeler, S. P.; Ritter, J. H.; Kang, L. L.; Dort, S.; Robichaud, A.; Head, R.; Holtzman, M. J.; Diamond, M. S. Publisher Correction: SARS-CoV-2 infection of human ACE2-transgenic mice causes severe lung inflammation and impaired function. *Nat. Immunol.* **2020**, *21*, 1470.

(79) Hsia, C. C. W.; Hyde, D. M.; Ochs, M.; Weibel, E. R. An official research policy statement of the American Thoracic Society/European Respiratory Society: standards for quantitative assessment of lung structure. *Am. J. Respir. Crit. Care Med.* **2010**, *181*, 394–418.

(80) Noske, G. D.; Nakamura, A. M.; Gawriljuk, V. O.; Fernandes, R. S.; Lima, G. M. A.; Rosa, H. V. D.; Pereira, H. D.; Zeri, A. C. M.; Nascimento, A. F. Z.; Freire, M.; Fearon, D.; Douangamath, A.; von Delft, F.; Oliva, G.; Godoy, A. S. A Crystallographic Snapshot of SARS-CoV-2 Main Protease Maturation Process. *J. Mol. Biol.* **2021**, *433*, No. 167118.

(81) ThermoFisher Z'-LYTE Screening Protocol and Assay Conditions. http://assets.thermofisher.com/TFS-Assets/BID/Methods-&-Protocols/20180123_SSBK_Customer_Protocol_and_Assay_Conditions.pdf.

(82) ThermoFisher Adapta Screening Protocol and Assay Conditions. http://assets.thermofisher.com/TFS-Assets/BID/Methods-&-Protocols/20180123_SSBK_Adapta_Customer_Protocol_and_Assay_Conditions.pdf.

(83) ThermoFisher LanthaScreen Eu Kinase Binding Assay Screening Protocol and Assay Conditions. http://assets.thermofisher.com/TFS-Assets/BID/Methods-&-Protocols/20180123_SSBK_LanthaScreen_Binding_Customer_Protocol_and_Assay_Conditions.pdf.